Temporal relationships between Mg-K mafic magmatism and catastrophic melting of the Variscan crust in the southern part of Velay Complex (Massif Central, France)

Simon Couzinié, Jean-François Moyen, Arnaud Villaros, Jean-Louis Paquette, Jane H. Scarrow, Christian Marignac

Original paper

Temporal relationships between Mg–K mafic magmatism and catastrophic melting of the Variscan crust in the southern part of Velay Complex (Massif Central, France)

Simon COUZINIÉ[1,2,3]*, Jean-François MOYEN[2,3], Arnaud VILLAROS[4,5,6], Jean-Louis PAQUETTE[2], Jane H. SCARROW[7], Christian MARIGNAC[8]

[1] *École Normale Supérieure de Lyon, 69364 Lyon Cedex 7, France; simon.couzinie@ens-lyon.org*
[2] *Laboratoire Magmas et Volcans, UMR 6524 CNRS, Université Blaise Pascal, Rue Kessler, 63038 Clermont-Ferrand, France*
[3] *Université Jean Monnet, 23 rue du Dr Paul Michelon, 42023 Saint-Étienne, France*
[4] *ISTO, UMR 7327, Univ. Orleans, F-45071 Orleans, France*
[5] *ISTO, UMR 7327, CNRS, F-45071 Orleans, France*
[6] *ISTO, UMR 7327, BRGM, F-45060 Orleans, France*
[7] *Department of Mineralogy and Petrology, Campus Fuentenueva, University of Granada, 18002 Granada, Spain*
[8] *UMR 7359 Géoressources, École des Mines, Campus ARTEM, CS 14 234, 54 042 Nancy Cedex, France*
* *Corresponding author*

Mg–K mafic intrusive rocks are commonly observed during the late stages of the evolution of orogenic belts. The Variscan French Massif Central has many outcrops of these rocks, locally called vaugnerites. Such magmas have a mantle-derived origin and therefore allow discussion of the role of mantle melting and crust–mantle interactions during late-orogenic processes. In the Southern Velay area of the French Massif Central, LA-ICPMS U–Pb dating on zircons and monazites from three vaugnerites and four coeval granites reveals that the two igneous suites formed simultaneously, at *c.* 305 Ma. This major igneous event followed after an early, protracted melting stage that lasted for 20–30 My and generated migmatites, but the melt was not extracted efficiently and therefore no granite plutons were formed. This demonstrates that widespread crustal anatexis, melt extraction and granite production were synchronous with the intrusion of vaugneritic mantle-derived melts in the crust. The rapid heating and subsequent melting of the crust led to upward flow of partially molten rocks, doming and collapse of the belt.

Keywords: vaugnerite, granite, U–Pb geochronology, Variscan, French Massif Central
Received: 17 May 2013; accepted: 19 November 2013; handling editor: M. Štemprok
The online version of this article (doi: 10.3190/jgeosci.155) contains supplementary electronic material.

1. Introduction

The Mg–K mafic magmatic suites correspond to a highly heterogeneous group of igneous rocks closely associated with post-collisional granitic suites (see review in Bonin 2004). Their relative scarcity but systematic occurrence throughout most orogens makes them particularly useful as markers to understand the evolution of the lithosphere at the end of major orogenic episodes. In the European Variscan belt for instance, various types of such rocks are diversely known as "vaugnerites" in the French Massif Central (Sabatier 1980; Michon 1987; Sabatier 1991), "durbachites" in the Vosges (Gagny 1979), Schwarzwald (Kober and Lippolt 1985) and Bohemian Massif (Holub 1997a, b; Janoušek et al. 1997; Gerdes et al. 2000; Kotková et al. 2003, 2010), shoshonites, appinites and lamprophyres in central Spain (Castro et al. 2003; Perini et al. 2004; Scarrow et al. 2008, 2009; Molina et al. 2012). Older examples include the Caledonian appinites (Fowler 1988; Bowes and Košler 1993; Fowler et al. 2008; Murphy 2013), and even the Archaean "sanukitoids" (Martin et al. 2010; Fowler and Rollinson 2012). Given that a mantle source has been invoked in the petrogenesis of all the above examples, these rocks can be used to address the question of mantle input, through mass and/or heat transfer, during crustal melting and granite production.

The vaugnerites of the French Massif Central are Mg–K-rich biotite-rich diorites. Although many petrological types are known (see review in Sabatier 1991), all examples share the same key characteristics: major minerals are biotite, plagioclase, hornblende, interstitial quartz and K-feldspar, minor clinopyroxene, and rare orthopyroxene (Montel 1988); accessory phases such as apatite, zircon, allanite and titanite are abundant (Montel and Weisbrod 1986). Vaugnerites usually crop out as intrusive bodies or enclaves in coeval felsic rocks (Sabatier 1991). They are well-exposed at the southern border of the Velay Complex, a large anatectic dome of migmatites cored by a heterogeneous, cordierite-bearing, S-type granite (Ledru et al. 2001).

The aim of this study is to constrain the temporal relationships between crustal melting and Mg–K mafic magmatism in the southern Velay, on the basis of field observations of vaugnerites coupled with U–Pb dating on zircon and monazite. Determining the chronological framework of the melting events allows us to constrain the crustal evolution in the region at the end of the Variscan orogeny.

2. Geological setting

The Variscan belt of Europe formed between *c.* 400 and 280 Ma as a result of the convergence between Laurussia, Gondwana and intervening microplates (Matte 1986; Edel 2001; Guy et al. 2011; Kroner et al. 2013). The French Massif Central is a Gondwana-derived microcontinent (Melleton et al. 2010) accreted to Laurussia in Devonian to Carboniferous times (e.g. von Raumer et al. 2003). A large portion of the Eastern French Massif Central is occupied by the Velay Complex, a *c.* 100 by 100 km migmatite dome (Lagarde et al. 1994; Ledru et al. 2001). A large volume of peraluminous granite forms its core (Williamson et al. 1992; Lagarde et al. 1994; Downes et al. 1997; Ledru et al. 2001), and cuts across the Early Carboniferous nappe stack (Faure et al. 2009 and references therein). The Southern Velay area experienced a polymetamorphic evolution during the Variscan orogeny, described as a succession of four major tectono-metamorphic events (Marignac et al. 1980; Montel et al. 1992). They affected two contrasting lithologies (Fig. 1): the Cambrian "Ardèchois" orthogneisses (R'Kha Chaham et al. 1990; Alexandre 2007; Melleton et al. 2010); and the possibly Precambrian to Ordovician "Cévenol" metasediments (Pin and Marini 1993; Caron 1994; Roger et al. 2004; Melleton et al. 2010).

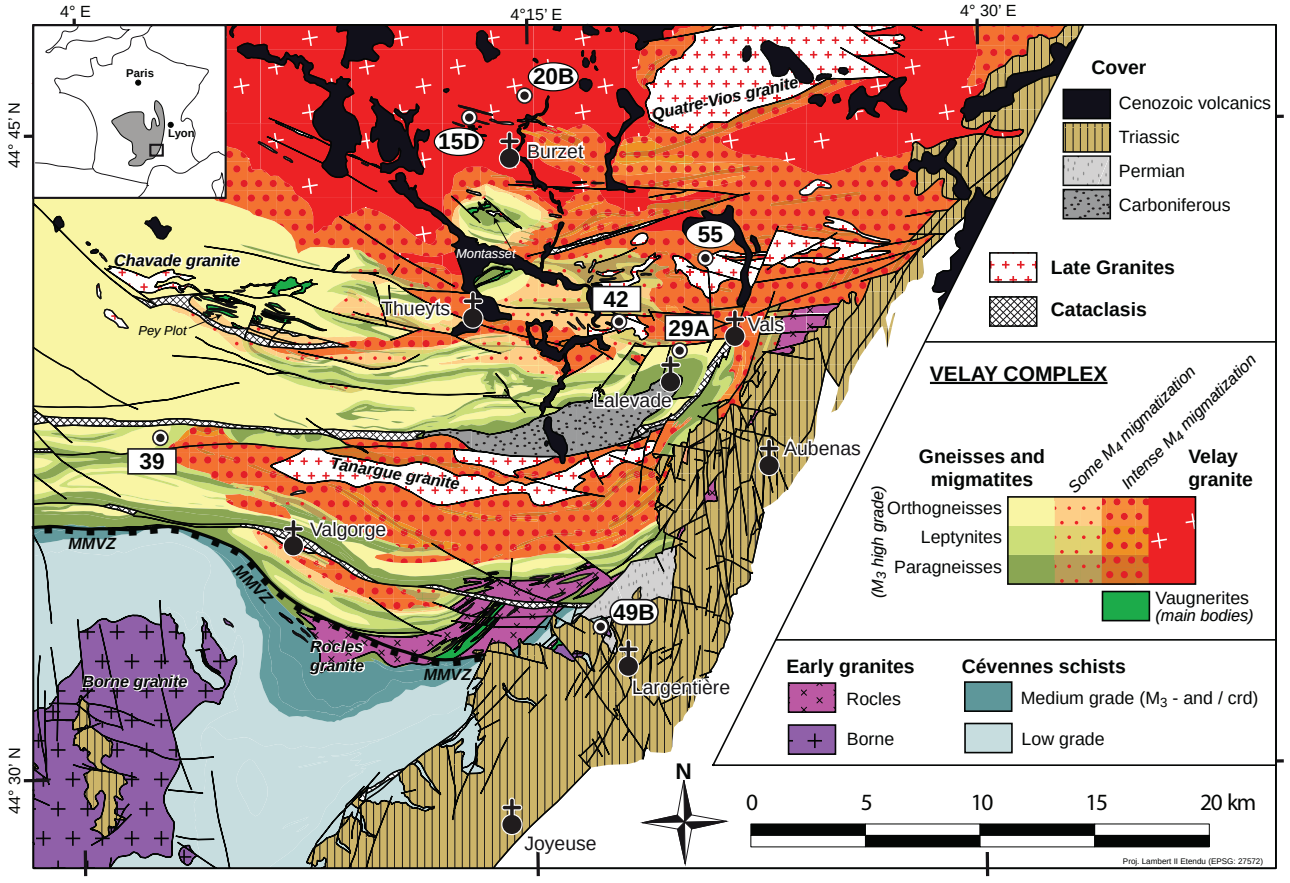

Fig. 1 Geological map of the Southern Velay region, adapted from Weisbrod (1970); 1/50 000 geological maps; and unpublished maps (ENSG mapping camps, 1970–1990s). Location map in inset, showing the study area in the south-eastern portion of the Variscan Massif Central (grey). The M_4 overprint is shown in orange (with red dots), superimposed on the yellow/green depicting the pre-M_4 lithologies (M_3 high-grade ortho- and paragneisses); the paragneisses of the "Cévenole" Series are the high-grade equivalents of the Cévennes schists, south of the MMVZ (Mylonitic Metamorphic Vellave Zone from Bouilhol et al. 2006). Only the largest vaugnerite bodies are shown here (in the Rocles granite, and at Pey Plot East of Chavade Pluton, cf. Ait Malek 1997); innumerable, 1 to 10 m bodies are found throughout the area. The location of geochronology samples is indicated on the map; peraluminous granite samples are ellipses (15D Peyron, 20B Velay, 55 Tanargue), vaugnerites rectangles (39 Loubaresse, 42 Meyras, 29A Pont-de-Bayzan) and metaluminous granites rectangles with rounded edges (49B Largentière). The Largentière granite is an outlier of the larger Borne Complex, to the west.

- D_1 is inferred from relicts in high-grade (eclogitic) units, mostly north and west of our study area (Lardeaux et al. 2001; Berger et al. 2010); the eclogitic metamorphism (M_1) is dated (U–Pb on zircons) at *c.* 410–430 Ma in various outcrops of the Massif Central (Pin and Lancelot 1982; Ducrot et al. 1983; Paquette et al. 1995; Berger et al. 2010).
- D_2 collisional nappe stacking linked to N–S compression (Marignac et al. 1980) caused the regional foliation. This event was associated with a syn-collisional MP–MT Barrovian metamorphism (M_2). Syn-metamorphic shearing has been dated at around 340–335 Ma (^{40}Ar– ^{39}Ar on biotite and amphibole), both south (Cévennes: Caron 1994) and north (Lyonnais: Costa and Rey 1995) of our study area.
- D_3 corresponds to NW–SE extension (Faure et al. 2009) associated with a LP–HT metamorphism M_3 that reached partial melting conditions with biotite remaining stable: $T < 750\,°C$, $P \geq 5$ kbar (Montel et al. 1992). In the field, rocks affected by the M_3 event are cordierite-free, stromatic migmatites developed at the expense of both ortho- and paragneisses. Monazite U–Th–Pb (EPMA) dating of anatectic paragneisses yielded ages of 329 ± 5 (Be Mezeme et al. 2006) and 323 ± 3 Ma (Cocherie et al. 2005). However, monazite dating by ID-TIMS gave a younger age of 314 ± 5 Ma (Mougeot et al. 1997). A HT shear zone, the Mylonitic Metamorphic Vellave Zone (MMVZ) (Bouilhol et al. 2006), developed during the M_3 event and brought the greenschist- to amphibolite-facies Cevennes schists in contact with high-grade metamorphic rocks from the "Ardèchoise" and "Cévenole" series. According to Bouilhol et al. (2006), the MMVZ reflects the uplift of the Velay Dome, but the timing of this ascent has remained disputed and in other studies the doming was associated with the M_4 event (Barbey et al. 1999; Ledru et al. 2001). The syntectonic (D_3) S-type Rocles granite (Weisbrod 1970) (Fig. 1) has been dated at 324 ± 4 (EPMA on monazite, Be Mezeme et al. 2007).
- D_4 is represented by NNE–SSW transtension. Regionally, it corresponded to the development of strike-slip shear zones such as the Sillon Houiller (Faure et al. 2009). In the northern part of the study area (Fig. 1), D_4 was associated with a M_4 metamorphism recording a regional temperature increase, leading to fluid-absent biotite melting in the cordierite stability field. The P–T estimates are $760 < T < 850\,°C$ and $2 < P < 5$ kbar (Montel et al. 1992). The M_4 migmatites are nebulitic to diatexitic and cordierite-bearing; it is sometimes possible to still recognize their protolith ("Ardèchois" orthogneisses or "Cévenol" paragneisses). The D_4/M_4 event was synchronous with emplacement of the main cordierite-bearing anatectic Velay granite which has been dated at 298 ± 8 (Rb–Sr whole-rock, Caen-Vachette et al. 1982) and 301 ± 5 Ma (U–Pb monazite, Mougeot et al. 1997).

The age of the Borne-Largentière I-type (sub-alkaline) granitic complex (Fig. 1) is unclear. A Rb–Sr whole-rock age of 315 ± 5 Ma was determined by Mialhe (1980), linking it with the D_3 event as proposed by Weisbrod (1970). On the other hand, two samples from the Mont-Lozère Complex, the western part of the Borne granite wrenched by the sinistral movement of the Villefort Fault, gave TIMS zircon ages of 303 ± 3 Ma (Brichau et al. 2008), 307 ± 5 Ma and 307 ± 11 Ma (François 2009), i.e., closer to D_4.

The whole area was affected by rapid uplift and cooling in the last stages of Variscan evolution as recorded by U–Pb apatite ages clustering around 290 Ma (Mougeot et al. 1997). The Velay granite and related M_4 migmatites are cross-cut by late granites belonging to two main suites, the Quatre-Vios and Tanargue granite, (Montel and Abdelghaffar 1993). The previously published Permian Rb–Sr ages (e.g. 274 ± 7 Ma for a Quatre-Vios granite, Caen-Vachette et al. 1982) are now believed to reflect late isotopic disturbance: the Montasset granite (Fig. 1) yielded pristine monazites with a LA-ICP-MS age of 307 ± 2 Ma, and fluid-altered monazites with scattered ages suggesting reopening of the isotopic system between 270 and 290 Ma (Didier et al. 2013).

3. Mg–K mafic intrusive rocks relationships to their hosts

Vaugnerites in the study area crop out in various settings (Fig. 2, and Electronic Appendix 1), depending on the nature of the host and its anatectic history.

3.1. Vaugnerites in orthogneisses

The vaugnerites intruding orthogneisses are generally meter-sized bodies (although they can occur in large swarms, such as at Pey Plot) and are fine- to medium-grained. They form lenses that are concordant with the regional foliation of ("Ardéchois") migmatitic orthogneisses (Fig. 2a). The cores of the bodies display an isotropic, probably magmatic texture whereas the rims have a cleavage that can be attributed to emplacement-related deformation. The vaugnerite bodies are commonly surrounded by small volumes of fine-grained granites, connected with surrounding leucosomes in the gneisses and therefore probably representing melt segregated from the partially molten gneisses. Interpenetrating textures and the feathered appearance of the contacts between vaugnerites and immediately surrounding fine-grained granites demonstrate that both were molten at the same time. Thus, our favoured interpretation is that the vaugnerites

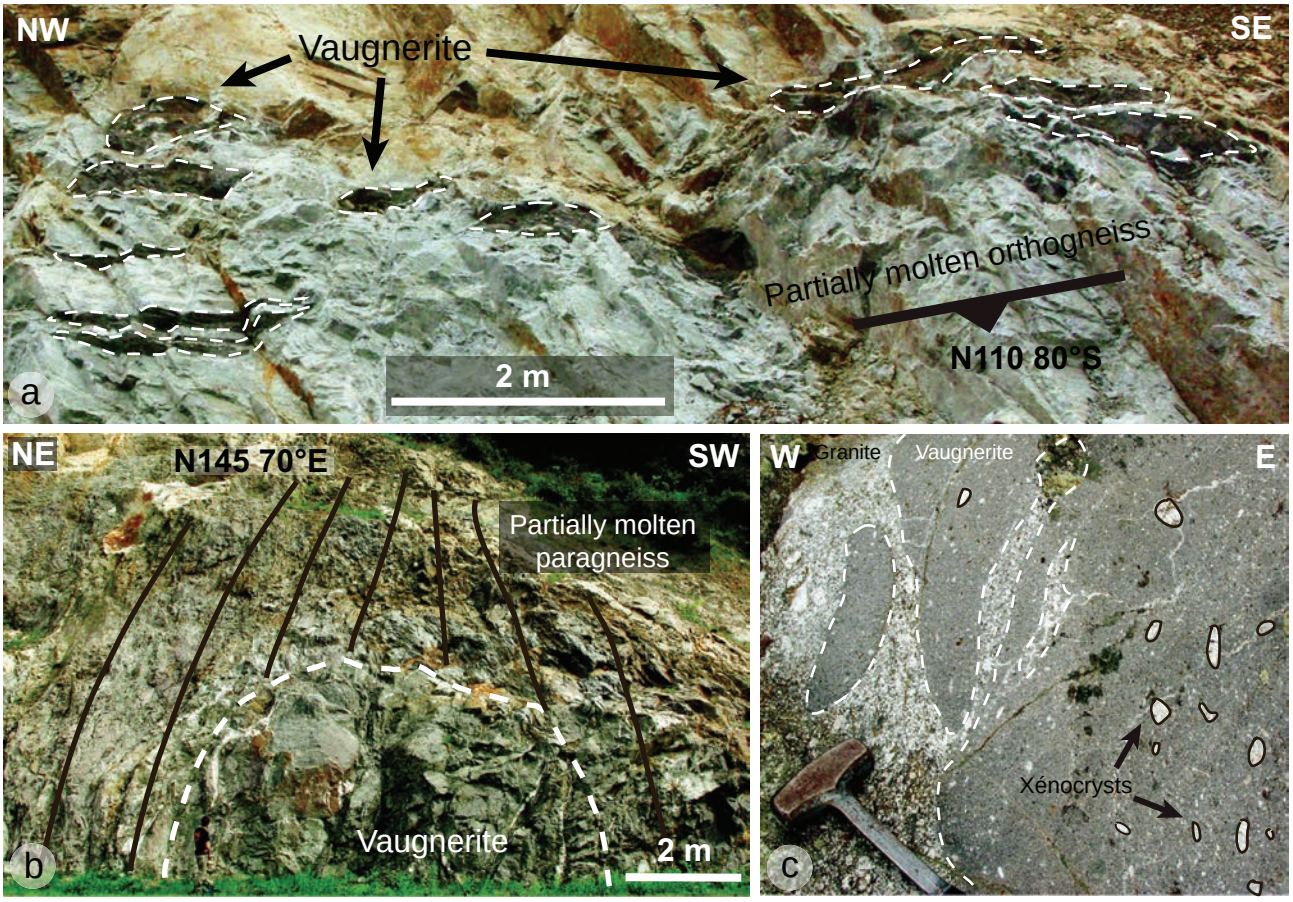

Fig. 2 Examples of vaugnerite outcrops. **a** – Vaugneritic lenses stretched in the foliation of migmatitic orthogneisses at Pont-de-Bayzan road cut (similar to our sample 29A). **b** – Intrusive vaugnerite forming a rounded enclave in diatexitic M_4 paragneisses, Pont-de-Bayzan. **c** – Mingling textures between a vaugnerite and the Largentière granite (our sample 49B), Ligne Valley. Hammer head 12 cm.

intruded a partially molten host, causing additional melting and/or melt segregation around the mafic bodies.

One sill of orthogneiss-hosted vaugnerite was dated by Ait Malek (1997) at Pey Plot using U–Pb TIMS on zircons; this gave an upper intercept age of 314 ± 3 Ma.

3.2. Vaugnerites in paragneisses

Vaugnerites intruding metatexitic to diatexitic paragneisses are medium- to coarse-grained stocks and sills (Fig. 2b), ranging from 2 to 50 m in length. These intrusive bodies cut across the regional foliation (Fig. 2b) or were emplaced in low-strain domains such as axial planes of folds (Ait Malek 1997). These vaugnerites are often surrounded by felsic, plagioclase- and biotite-rich, sometimes tourmaline-bearing, pegmatoids. The outcrop shape of vaugnerites correlates with the type of migmatites in which they intrude: vaugnerites in cordierite-free, M_3 migmatites (mostly metatexites) tend to form sills. This is the case for the Loubaresse sill (our sample 39, Fig. 1), previously dated by U–Pb TIMS on zircons by Ait Malek (1997) at 313 ± 3 Ma (upper intercept). In contrast, vaugnerites in M_4 cordierite-bearing migmatites (diatexites commonly) often form rounded masses, for example at Pont-de-Bayzan (figure 2b, our sample 29A, Fig. 1) or Meyras (our sample 42, Fig. 1), which gave an age of 308 ± 6 Ma using TIMS on zircons (Ait Malek 1997).

3.3. Vaugnerites associated with granitic bodies

Meter-size vaugneritic enclaves are enclosed by most granites in the area. The coeval ascent and crystallization of mafic and felsic melts are evidenced by lobate contacts and intricate shapes (Fig. 2c). Such mingling features are well-exposed north-west of Burzet where a fine-grained vaugnerite, the “Peyron diorite” (Didier et al. 1987) and a coeval biotite-bearing granite cut across the heterogeneous cordierite-bearing Velay granite (our sample 15D, Fig. 1). Vaugnerite is also found within other late granites (such as the Tanargue granite, our sample 55, Fig. 1) or the main, heterogeneous Velay granite (sample 20B, Fig. 1). Finally, in the Ligne Valley, just north of Largentière, K-feldspar megacryst-bearing vaugnerites

Tab. 1 Summary of samples and geochronological results. Latitude and longitude in decimal degrees, WGS84.

Sample number	Location			Rock type	Zircon magmatic age	Monazite magmatic age
	Place name	Latitude	Longitude			
SGC12 15D	Peyron	44.75042	4.22173	Late granite (unnamed granite surrounding Peyron diorite)	undefined	303.7 ± 3.1 Ma
SGC12 20B	Burzet	44.78277	4.25688	Velay granite	undefined	305.9 ± 1.4 Ma
SGC12 29A	Pont de Bayzan	44.65678	4.29928	Vaugnerite	294.4 ± 3.9 Ma	–
SGC12 39	Loubaresse	44.60045	4.07053	Vaugnerite	307.4 ± 1.8 Ma	–
SGC12 42	Meyras	44.67262	4.27383	Vaugnerite	305.8 ± 2.3 Ma	–
SGC12 49B	Largentière	44.5548	4.28738	Porphyritic granite (Borne-Largentière)	304.1 ± 6.3 Ma	–
SGC12 55	Chadenet	44.69342	4.35143	Late granite (Tanargue suite)	303.9 ± 6.5 Ma	–

(resulting from mingling between ordinary vaugnerites and porphyritic granite) and the porphyritic potassic amphibole-bearing Largentière granite (Fig. 1) intrude the M_3 amphibolite-facies Cévennes micaschists (Palm 1957). The Largentière granite is similar to the Borne Pluton and is regarded as an offshoot of this (Weisbrod 1970); indeed the Borne granite has very common mafic microgranular enclaves of vaugneritic composition (Mialhe 1980). The Largentière vaugnerites and granites crop out in a 400 meters long polished river bed displaying many examples of the mingling textures (Fig. 2c).

4. U–Pb geochronology

4.1. Sample selection and techniques

Seven samples were selected for LA ICP-MS geochronology (Tab. 1), with the aim of constraining the timing of vaugnerite emplacement. Therefore, we dated either vaugnerites directly or granites demonstrably coeval with the vaugnerites. Details of the field relationships and sample descriptions are given in Electronic Appendix 1. A vaugnerite (29A) stretched in the foliation of a migmatitic orthogneiss at Pont-de-Bayzan (Fig. 1) was chosen to constrain the emplacement age of the most deformed intrusions, presumed to be the oldest in the study area. The Loubaresse sill (39) and a rounded vaugnerite at Meyras (42), both corresponding to samples previously dated by Ait Malek (1997), were selected as representative of the two main types of paragneiss-hosted vaugnerites; this also allowed comparison of our LA-ICP-MS results with previously published TIMS data. Four granites, closely associated with vaugnerites, were also dated (Fig. 1): a heterogeneous cordierite-bearing Velay granite (20B) displaying ductile interactions with a vaugnerite sampled north of Burzet; a biotite–cordierite-bearing slightly porphyritic Tanargue granite (55) closely associated with a vaugnerite cropping out in Chadenet; a biotite-bearing Peyron granite (15D) that intruded the Velay granite and was synchronous with the "Peyron diorite" (Didier et al. 1987). Finally, biotite-bearing porphyritic Largentière granite (49B) from the Ligne Valley near Largentière was selected to date the coeval vaugneritic intrusion.

Rock samples were crushed using standard techniques (jaw crusher, disc mill) and the powder fraction <500 μm was kept. Zircons and monazites were concentrated using heavy liquids (tetrabromoethane and diiodomethane), an isodynamic Frantz separator, and then hand-picked under a binocular microscope, mounted in epoxy resin, and polished to an equatorial grain section. Analytical work was carried out in the Laboratoire Magmas et Volcans (Clermont-Ferrand). Minerals were imaged by cathodoluminescence using a Jeol JSM-5910 MEB and U–Pb analyses were conducted *in situ* by LA ICP-MS with an Agilent 7500ICP-MS coupled to a Resonetics M-50E 193 nm ArF Excimer laser system. Ablation spot diameters of 26 μm and 7 μm with repetition rates of 3 Hz and 1 Hz were used for zircon and monazite, respectively. Data were corrected for U–Pb fractionation and the mass bias by standard bracketing with repeated measurements of the GJ-1 zircon (Jackson et al. 2004) and the Moacyr monazite standards (Gasquet et al. 2010). Repeated analyses of the same standards treated as unknowns were used to control the reproducibility and accuracy of the corrections. Data reduction was carried out with the GLITTER® software package developed by Macquarie Research Ltd. (Jackson et al. 2004). Concordia ages

and diagrams were generated using Isoplot (Ludwig 2008). Further information on the instrumentation and the analytical technique is given in Hurai et al (2010).

4.2. Results

Orthogneiss-hosted **vaugnerite 29A (Pont de Bayzan)** yielded only a limited amount of small (around 50 µm), yellowish U-rich zircons (*c.* 2,000–5,000 ppm). Consequently, most analyses are highly discordant and contain large amounts of common Pb (Tab. 2). A regression line can be established by the combination of the oldest and least discordant points together with discordant data toward common Pb composition at about 300 Ma. In the Tera-Wasserburg diagram (Tera and Wasserburg 1972; Fig. 3a), the data define a trend with a lower intercept at 294 ± 3.9 Ma.

Samples 39 (Loubaresse) and **42 (Meyras)** yielded more zircon grains (Tab. 2). The *c.* 300–700 ppm U contents and a larger number of data allow better definition of the crystallization ages: 307.4 ± 1.8 Ma for Loubaresse (39) and 305.8 ± 2.3 Ma for Meyras (42) (Fig. 3b–c).

A similar, complex pattern where the analytical points are characterized by discordance associated to common Pb contribution is observed in the metaluminous **Largentière granite 49B** (Fig. 4a). As for 29A, we interpret the analytical data as defining a discordia with a lower intercept age of 304.1 ± 6.3 Ma. The latter is similar, within error, to the ages obtained previously for the Mont-Lozère Complex (Brichau et al. 2008; François 2009), confirming that the Largentière granite is part of the Lozère-Borne Pluton, the age of which appears to be younger than the previously assumed D_3 timing (Weisbrod 1970). No zircon inheritance is recorded in this granite in accordance with its metaluminous character (Bea et al. 2006).

Cathodoluminescence imaging of zircons from the peraluminous **Tanargue granite (sample 55)** reveals the presence of bright cores surrounded by darker rims, interpreted as inherited cores and magmatic overgrowths during granite formation. The data allow better definition of a discordia line (Fig. 4b), with a lower intercept at 303.9 ± 6.5 Ma, that we interpret as the crystallization age.

Both the main cordierite-bearing **Velay granite (20B),** and the apparently cross-cutting **Peyron granite (15D)**, also have inherited cores and younger rims. Although some zircon analyses tend to be more concordant than in the other samples, the points scatter along the concordia (Fig. 4c and d) and do not allow definition of a proper crystallization age. On the other hand, euhedral, yellowish monazites were extracted from both samples and provided well-constrained, concordant U–Th–Pb ages of, respectively, 305.9 ± 1.4 and 303.7 ± 3.1 Ma (Fig. 5).

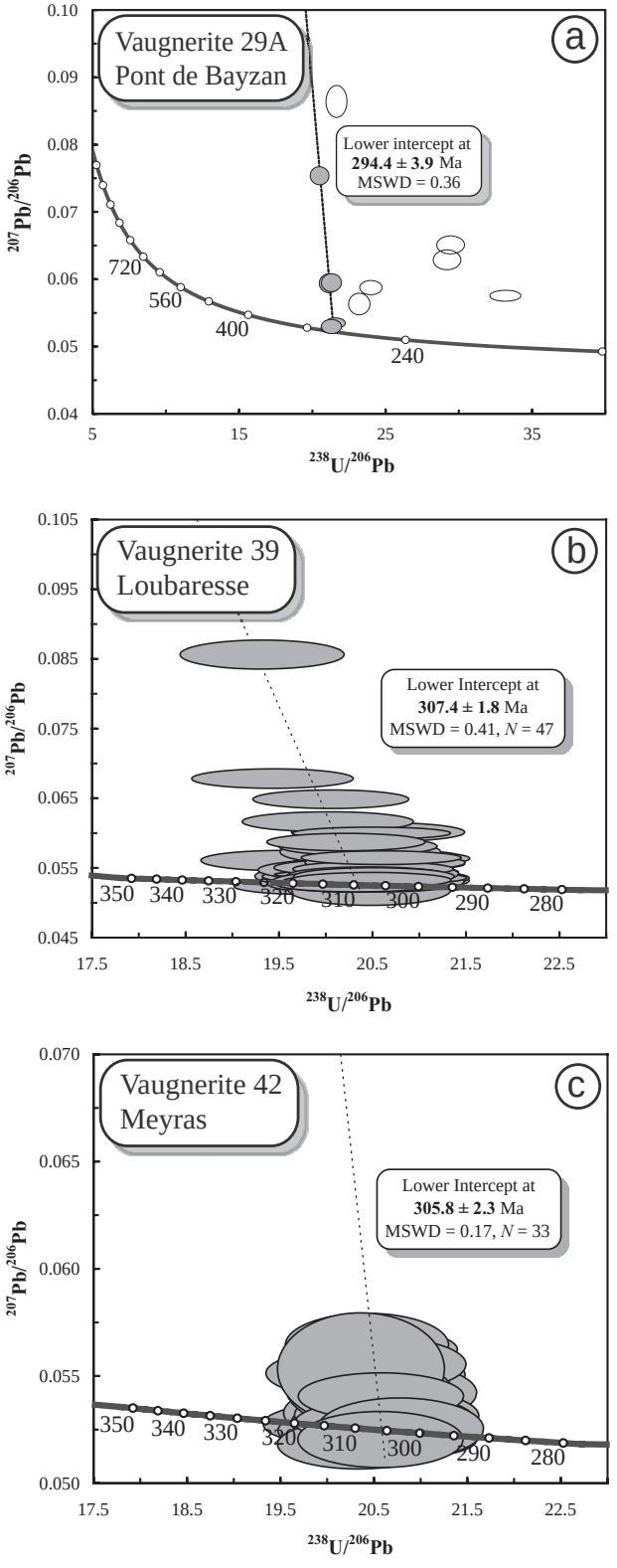

Fig. 3 Tera-Wasserburg diagrams for the three samples of vaugnerite from this study. All ellipses are represented at 2σ level and also all ages are quoted at 2σ level. Grey ellipses show the data used for age regression. Ages are calculated and figures plotted using Isoplot (Ludwig 2008).

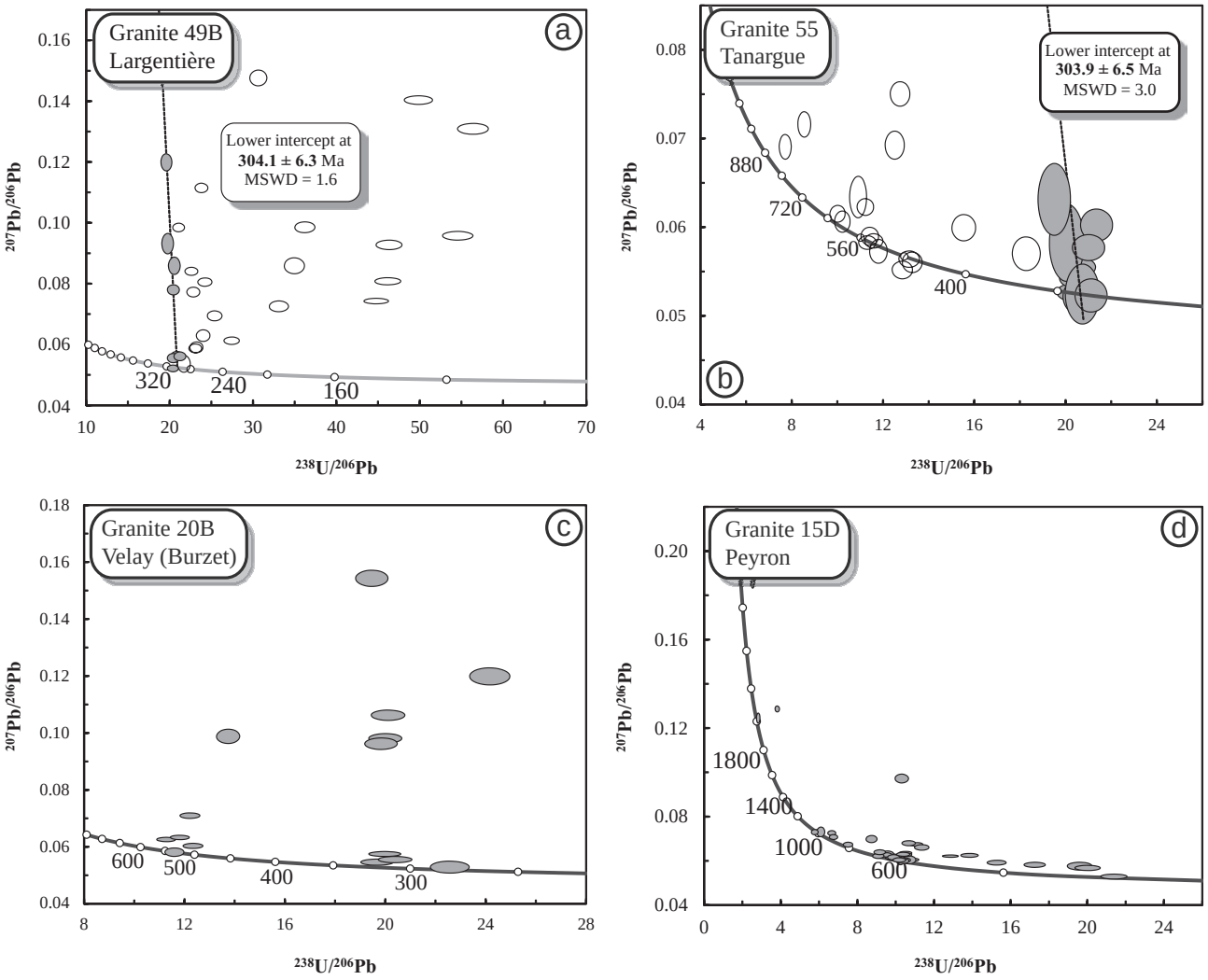

Fig. 4 Tera-Wasserburg diagrams for the four granite samples from this study. Grey ellipses show the data used for age regression.

Inherited cores range in age from 470 to 2100 Ma; the meaning of distinct inheritance patterns in each of the granitic sample is discussed in section 5.3.

5. Discussion

5.1. Chronological framework of the mafic magmatism

Vaugneritic magmatism has been dated either directly, or by using coeval felsic magmas, which allows definition of a better-constrained age. We emphasize that, in this study, the granite samples were taken in close vicinity (< 1 m) to the "target" mafic bodies, with clear magmatic contacts (Fig. 2 and Appendix 1) and common mingling features. The ages obtained in either case are very consistent and indistinguishable within error (from 303.7 ± 3.1 to 307.4 ± 1.8 Ma).

Ages of *c.* 315 Ma previously obtained by ID-TIMS on vaugnerites from the Southern Velay (Ait Malek 1997) could not be reproduced in this study. We re-dated two of the bodies studied by Ait-Malek (1997), at Loubaresse (39) and Meyras (42). At Loubaresse, we found a younger age of 307.4 ± 1.8 Ma. We believe the older 313 ± 3 Ma age to be an artefact of the ID-TIMS method: the dissolution of large zircon fractions may not allow unravelling of complex patterns of lead loss such as observed in the vaugnerites. Indirect confirmation of this interpretation is provided by the *c.* 305 Ma age obtained by Ait Malek on coeval granites at Loubaresse. At Meyras on the other hand, our age (305.8 ± 2.3 Ma) is indistinguishable from the TIMS age (308 ± 6 Ma) of Ait Malek (1997). Collectively the evidence suggests that the emplacement of the vaugnerite–granite association occurred at 305 Ma, both at Loubaresse and Meyras – and elsewhere in the Southern Velay.

The meaning of the Permian age (294 ± 3.9 Ma) at Pont de Bayzan (sample 29A) is rather unclear. As a re-

Tab. 2 LA-ICP-MS U–Pb data for monazite and zircon from seven samples. Uncertainties are given at two sigma level.

	Concentrations				Isotopic ratios				Age (Ma)	
Spot	**Pb ppm[1]**	**Th ppm[1]**	**U ppm[1]**	**Th/U**	**$^{207}Pb/^{235}U^{2}$**	**± 2σ**	**$^{206}Pb/^{238}U^{2}$**	**± 2σ**	**$^{206}Pb/^{238}U$**	**± 2σ**
Pont-de-Bayzan vaugnerite 29A zircons										
29A/1	125	3209	2343	1.37	0.3352	0.0118	0.04309	0.00113	271.9	7.0
29A/2	292	5276	9105	0.58	0.2393	0.0067	0.03012	0.00078	191.3	4.8
29A/3	111	2388	1845	1.29	0.5506	0.0191	0.04616	0.00123	290.9	7.5
29A/4	98	1331	1984	0.67	0.3424	0.0097	0.04640	0.00120	292.4	7.4
29A/5	130	1637	2601	0.63	0.3434	0.0096	0.04718	0.00120	297.2	7.5
29A/6	170	1809	4884	0.37	0.2974	0.0097	0.03425	0.00090	217.1	5.6
29A/7	114	1034	2733	0.38	0.3379	0.0100	0.04166	0.00108	263.1	6.7
29A/8	106	1918	1840	1.04	0.5081	0.0152	0.04889	0.00128	307.7	7.9
29A/9	98	2080	1821	1.14	0.3879	0.0127	0.04734	0.00125	298.2	7.7
29A/10	119	3186	2130	1.50	0.3860	0.0122	0.04702	0.00123	296.2	7.6
29A/11	137	956	2987	0.32	0.3439	0.0105	0.04703	0.00123	296.3	7.6
29A/12	197	4654	5198	0.90	0.3052	0.0096	0.03396	0.00090	215.3	5.6
Loubaresse vaugnerite 39 zircons										
39/1	23	303	409	0.74	0.3608	0.0148	0.05025	0.00183	316.0	11.3
39/2	23	267	376	0.71	0.4801	0.0193	0.05146	0.00188	323.5	11.5
39/3	55	1291	782	1.65	0.3567	0.0140	0.04905	0.00180	308.7	11.0
39/4	31	610	472	1.29	0.3663	0.0166	0.04963	0.00183	312.3	11.3
39/5	17	177	291	0.61	0.3938	0.0167	0.05117	0.00188	321.7	11.6
39/6	44	996	615	1.62	0.3580	0.0144	0.04888	0.00180	307.6	11.0
39/7	28	46	600	0.08	0.3544	0.0143	0.04893	0.00180	307.9	11.1
39/8	22	46	471	0.10	0.3535	0.0146	0.04850	0.00178	305.3	11.0
39/9	20	87	425	0.21	0.3579	0.0151	0.04901	0.00183	308.4	11.2
39/10	30	631	431	1.46	0.4017	0.0168	0.04863	0.00180	306.1	11.1
39/11	42	924	611	1.51	0.3645	0.0149	0.04942	0.00183	311.0	11.3
39/12	17	117	337	0.35	0.3717	0.0163	0.04951	0.00185	311.5	11.3
39/13	18	173	341	0.51	0.3562	0.0156	0.04928	0.00183	310.1	11.3
39/14	35	619	480	1.29	0.6111	0.0258	0.05175	0.00193	325.3	11.9
39/15	34	338	650	0.52	0.3563	0.0149	0.04853	0.00180	305.5	11.1
39/16	26	128	498	0.26	0.4227	0.0178	0.04994	0.00188	314.1	11.5
39/17	18	134	345	0.39	0.3651	0.0139	0.04870	0.00165	306.5	10.2
39/18	24	45	534	0.08	0.3694	0.0135	0.04847	0.00165	305.1	10.1
39/19	10	102	191	0.53	0.3475	0.0175	0.04884	0.00170	307.4	10.5
39/20	22	201	422	0.48	0.3583	0.0135	0.04908	0.00168	308.9	10.3
39/21	83	2193	1056	2.08	0.3654	0.0128	0.04926	0.00168	310.0	10.3
39/22	28	76	597	0.13	0.3734	0.0136	0.04882	0.00165	307.3	10.2
39/23	21	92	434	0.21	0.3590	0.0139	0.04902	0.00168	308.5	10.3
39/24	21	62	458	0.14	0.3624	0.0137	0.04860	0.00165	305.9	10.2
39/25	24	457	377	1.21	0.3738	0.0141	0.04834	0.00165	304.3	10.1
39/26	20	298	345	0.86	0.3723	0.0142	0.04884	0.00168	307.4	10.3
39/27	19	368	302	1.22	0.3670	0.0142	0.04881	0.00168	307.2	10.3
39/28	20	385	310	1.24	0.3528	0.0146	0.04850	0.00168	305.3	10.2
39/29	26	208	513	0.41	0.3557	0.0130	0.04841	0.00165	304.7	10.1
39/30	39	931	546	1.71	0.3792	0.0137	0.04864	0.00165	306.2	10.2
39/31	13	218	207	1.05	0.3860	0.0165	0.04908	0.00170	308.9	10.4
39/32	15	63	319	0.20	0.3723	0.0142	0.04929	0.00168	310.2	10.4
39/33	49	1022	723	1.41	0.3587	0.0132	0.04905	0.00168	308.7	10.3
39/34	9.7	146	167	0.88	0.3611	0.0150	0.04863	0.00168	306.1	10.3
39/35	20	215	346	0.62	0.4444	0.0169	0.04985	0.00170	313.6	10.5
39/36	31	510	515	0.99	0.3708	0.0142	0.04845	0.00165	305.0	10.2
39/37	33	446	590	0.76	0.3669	0.0139	0.04875	0.00168	306.8	10.2
39/38	27	500	418	1.20	0.3921	0.0152	0.04915	0.00168	309.3	10.3
39/39	30	252	568	0.44	0.3762	0.0139	0.04855	0.00165	305.6	10.2
39/40	24	395	402	0.98	0.3619	0.0140	0.04890	0.00168	307.8	10.3
39/41	49	918	768	1.20	0.4020	0.0144	0.04880	0.00165	307.2	10.2
39/42	19	365	289	1.26	0.3584	0.0150	0.04930	0.00170	310.2	10.4
39/43	24	222	467	0.48	0.3573	0.0131	0.04900	0.00168	308.4	10.3
39/44	25	502	382	1.31	0.3989	0.0154	0.04946	0.00170	311.2	10.4
39/45	34	419	600	0.70	0.3541	0.0131	0.04917	0.00168	309.4	10.3
39/46	16	74	347	0.21	0.3595	0.0142	0.04873	0.00168	306.7	10.3
39/47	25	397	433	0.92	0.3565	0.0137	0.04882	0.00168	307.3	10.3

Tab. 2 Continued

	Concentrations				Isotopic ratios				Age (Ma)	
Spot	**Pb ppm[1]**	**Th ppm[1]**	**U ppm[1]**	**Th/U**	**$^{207}Pb/^{235}U^{2}$**	**± 2σ**	**$^{206}Pb/^{238}U^{2}$**	**± 2σ**	**$^{206}Pb/^{238}U$**	**± 2σ**
Meyras vaugnerite 42 zircons										
42/1	18	169	363	0.46	0.3485	0.0133	0.04824	0.00165	303.7	10.2
42/2	22	222	416	0.53	0.3614	0.0136	0.04849	0.00165	305.2	10.2
42/3	17	168	328	0.51	0.3747	0.0143	0.04937	0.00170	310.7	10.4
42/4	23	270	431	0.63	0.3591	0.0136	0.04945	0.00170	311.1	10.4
42/5	30	438	558	0.78	0.3556	0.0132	0.04843	0.00165	304.9	10.2
42/6	13	110	266	0.41	0.3523	0.0149	0.04890	0.00168	307.8	10.4
42/7	9.1	77	180	0.43	0.3706	0.0156	0.04889	0.00168	307.7	10.4
42/8	13	109	265	0.41	0.3522	0.0156	0.04850	0.00168	305.3	10.3
42/9	33	564	566	1.00	0.3549	0.0132	0.04885	0.00168	307.5	10.3
42/10	30	423	544	0.78	0.3511	0.0130	0.04841	0.00165	304.8	10.2
42/11	19	182	378	0.48	0.3542	0.0135	0.04907	0.00168	308.8	10.3
42/12	11	80	218	0.37	0.3587	0.0144	0.04891	0.00168	307.8	10.3
42/13	67	1054	1173	0.90	0.3611	0.0129	0.04874	0.00165	306.8	10.2
42/14	28	385	497	0.78	0.3767	0.0139	0.04864	0.00165	306.2	10.2
42/15	11	28	239	0.12	0.3743	0.0149	0.04905	0.00168	308.7	10.4
42/16	17	161	334	0.48	0.3541	0.0138	0.04871	0.00168	306.6	10.3
42/17	13	63	267	0.24	0.3516	0.0138	0.04824	0.00165	303.7	10.2
42/18	50	775	842	0.92	0.3631	0.0132	0.04880	0.00168	307.1	10.3
42/19	15	113	292	0.39	0.3559	0.0140	0.04862	0.00168	306.0	10.3
42/20	13	19	288	0.07	0.3798	0.0154	0.04887	0.00168	307.6	10.4
42/21	45	554	822	0.67	0.3673	0.0139	0.04846	0.00165	305.1	10.2
42/22	21	220	395	0.56	0.3597	0.0145	0.04820	0.00165	303.4	10.2
42/23	19	166	385	0.43	0.3521	0.0138	0.04815	0.00165	303.1	10.2
42/24	23	270	448	0.60	0.3704	0.0143	0.04843	0.00165	304.9	10.2
42/25	22	265	386	0.69	0.3498	0.0135	0.04908	0.00168	308.9	10.3
42/26	12	75	254	0.30	0.3636	0.0154	0.04875	0.00168	306.8	10.3
42/27	23	228	432	0.53	0.3518	0.0135	0.04825	0.00165	303.8	10.1
42/28	7	51	149	0.34	0.3734	0.0197	0.04902	0.00173	308.5	10.6
42/29	26	274	481	0.57	0.3535	0.0134	0.04861	0.00168	306.0	10.2
42/30	33	528	585	0.90	0.3451	0.0128	0.04819	0.00165	303.4	10.2
42/31	25	398	439	0.91	0.3611	0.0139	0.04852	0.00168	305.4	10.3
42/32	12	25	272	0.09	0.3474	0.0143	0.04804	0.00165	302.5	10.2
42/33	18	291	328	0.89	0.3475	0.0140	0.04853	0.00168	305.5	10.3
Largentière granite 49B zircons										
49B/1	6	11	11	1.03	16.1352	0.5480	0.17678	0.00563	1049.4	30.8
49B/2	11	97	228	0.42	0.3417	0.0177	0.04601	0.00135	290.0	8.3
49B/3	16	189	259	0.73	0.6530	0.0268	0.05081	0.00148	319.5	9.0
49B/4	26	538	489	1.10	0.3513	0.0119	0.04329	0.00120	273.2	7.4
49B/5	8	45	26	1.72	8.4903	0.2830	0.11039	0.00340	675.0	19.7
49B/6	8	40	28	1.42	7.5529	0.2377	0.10387	0.00305	637.0	17.9
49B/7	13	183	245	0.75	0.3729	0.0129	0.04806	0.00133	302.6	8.2
49B/8	30	526	613	0.86	0.3513	0.0128	0.04302	0.00120	271.5	7.4
49B/9	266	1050	11913	0.09	0.2294	0.0066	0.02233	0.00060	142.3	3.9
49B/10	15	199	309	0.64	0.3620	0.0137	0.04161	0.00118	262.8	7.2
49B/11	32	408	629	0.65	0.4673	0.0152	0.04377	0.00123	276.2	7.5
49B/12	82	1323	2398	0.55	0.3026	0.0104	0.03017	0.00085	191.6	5.3
49B/13	56	507	1244	0.41	0.4585	0.0141	0.04124	0.00113	260.5	7.0
49B/14	170	2181	6832	0.32	0.3886	0.0112	0.02005	0.00055	128.0	3.5
49B/15	33	258	590	0.44	0.6448	0.0192	0.04741	0.00130	298.6	8.0
49B/16	51	922	1504	0.61	0.3393	0.0128	0.02860	0.00080	181.8	5.1
49B/17	93	1611	3742	0.43	0.2766	0.0086	0.02159	0.00060	137.7	3.8
49B/18	25	121	410	0.29	0.8463	0.0287	0.05119	0.00143	321.8	8.8
49B/19	109	254	2297	0.11	0.6462	0.0192	0.04197	0.00115	265.1	7.1
49B/20	276	9763	11133	0.88	0.3202	0.0093	0.01772	0.00048	113.2	3.1
49B/21	23	282	389	0.72	0.5784	0.0230	0.04880	0.00140	307.1	8.6
49B/22	19	166	369	0.45	0.3774	0.0132	0.04919	0.00135	309.6	8.4
49B/23	38	277	927	0.30	0.3779	0.0128	0.03936	0.00110	248.8	6.8
49B/24	81	841	1898	0.44	0.6667	0.0207	0.03267	0.00090	207.2	5.6
49B/25	132	6917	5571	1.24	0.2423	0.0072	0.01832	0.00050	117.1	3.2
49B/26	35	479	597	0.80	0.5281	0.0173	0.04907	0.00135	308.8	8.3

Tab. 2 Continued

	Concentrations				Isotopic ratios				Age (Ma)	
Spot	**Pb ppm[1]**	**Th ppm[1]**	**U ppm[1]**	**Th/U**	**$^{207}Pb/^{235}U^{2}$**	**± 2σ**	**$^{206}Pb/^{238}U^{2}$**	**± 2σ**	**$^{206}Pb/^{238}U$**	**± 2σ**
49B/27	146	2951	6085	0.48	0.2416	0.0073	0.02164	0.00060	138.0	3.7
49B/28	152	4881	3177	1.54	0.3084	0.0099	0.03644	0.00100	230.7	6.2
49B/29	19	174	366	0.48	0.3545	0.0116	0.04924	0.00135	309.8	8.3
49B/30	25	142	519	0.27	0.3664	0.0127	0.04727	0.00130	297.7	8.0
49B/31	157	1600	4932	0.32	0.3757	0.0116	0.02759	0.00075	175.4	4.8
49B/32	54	219	1146	0.19	0.5134	0.0154	0.04418	0.00120	278.7	7.5
Tanargue granite 55 zircons										
55/1	25	141	507	0.28	0.3577	0.0113	0.04926	0.00135	310.0	8.3
55/2	21	119	441	0.27	0.3480	0.0114	0.04856	0.00133	305.7	8.2
55/3	38	32	468	0.07	0.7115	0.0220	0.08741	0.00240	540.2	14.2
55/4	19	136	385	0.35	0.3670	0.0119	0.04902	0.00135	308.5	8.3
55/5	31	155	648	0.24	0.3712	0.0117	0.04851	0.00133	305.3	8.2
55/6	31	77	312	0.25	0.8480	0.0255	0.09991	0.00273	613.9	16.0
55/7	26	30	359	0.08	0.5920	0.0180	0.07603	0.00208	472.4	12.4
55/8	18	92	234	0.39	0.5819	0.0187	0.07524	0.00205	467.6	12.3
55/9	23	48	300	0.16	0.5922	0.0184	0.07777	0.00213	482.8	12.7
55/10	60	49	743	0.07	0.6952	0.0204	0.08617	0.00233	532.8	13.9
55/11	49	44	598	0.07	0.7101	0.0208	0.08827	0.00240	545.3	14.2
55/12	23	76	277	0.28	0.7625	0.0251	0.07980	0.00218	494.9	13.1
55/13	23	82	281	0.29	0.8112	0.0252	0.07840	0.00213	486.6	12.8
55/14	5	100	80	1.26	0.4010	0.0275	0.04991	0.00155	314.0	9.5
55/15	41	314	393	0.80	0.7646	0.0227	0.08898	0.00240	549.5	14.3
55/16	19	86	182	0.47	0.8186	0.0258	0.09780	0.00265	601.5	15.6
55/17	37	45	297	0.15	1.2343	0.0394	0.12951	0.00353	785.1	20.1
55/18	16	33	178	0.18	0.8016	0.0330	0.09160	0.00258	565.0	15.2
55/19	46	116	374	0.31	1.1537	0.0367	0.11680	0.00318	712.1	18.3
55/20	26	93	481	0.19	0.4303	0.0166	0.05467	0.00150	343.1	9.2
55/21	28	117	431	0.27	0.5322	0.0181	0.06434	0.00175	401.9	10.6
55/22	73	727	1434	0.51	0.3891	0.0143	0.04684	0.00128	295.1	7.9
55/23	22	276	184	1.50	0.6697	0.0223	0.08470	0.00230	524.1	13.7
55/24	6	76	118	0.64	0.3499	0.0146	0.04862	0.00135	306.0	8.3
55/25	5	55	96	0.57	0.3491	0.0211	0.04824	0.00143	303.7	8.8
55/26	19	387	305	1.27	0.3790	0.0130	0.04761	0.00130	299.8	8.0
55/27	9	150	149	1.01	0.3419	0.0137	0.04738	0.00130	298.4	8.0
55/28	5	58	76	0.77	0.4467	0.0270	0.05130	0.00155	322.5	9.5
Velay (Burzet) granite 20B zircons										
20B/1	90	266	1617	0.16	0.6773	0.0207	0.05000	0.00135	314.5	8.4
20B/2	51	30	602	0.05	0.7676	0.0223	0.08868	0.00240	547.7	14.2
20B/3	30	92	532	0.17	0.7297	0.0223	0.04972	0.00135	312.8	8.3
20B/4	64	274	1261	0.22	0.3840	0.0120	0.05083	0.00138	319.6	8.4
20B/5	23	88	556	0.16	0.3239	0.0137	0.04429	0.00123	279.4	7.6
20B/6	73	142	1142	0.12	1.0941	0.0342	0.05136	0.00140	322.9	8.6
20B/7	64	265	1333	0.20	0.3764	0.0118	0.04903	0.00133	308.6	8.1
20B/8	22	28	287	0.10	0.9927	0.0344	0.07274	0.00200	452.7	12.0
20B/9	218	38	2893	0.01	0.6764	0.0197	0.08102	0.00215	502.2	12.8
20B/10	356	32	4480	0.01	0.7398	0.0210	0.08451	0.00223	523.0	13.3
20B/11	277	54	3496	0.02	0.8015	0.0230	0.08176	0.00215	506.6	12.9
20B/12	78	335	1548	0.22	0.3974	0.0116	0.05003	0.00133	314.7	8.1
20B/13	15	85	166	0.51	0.6929	0.0234	0.08612	0.00230	532.5	13.7
20B/14	48	188	1039	0.18	0.6853	0.0234	0.04138	0.00113	261.4	7.0
20B/15	57	172	1052	0.16	0.6695	0.0213	0.05039	0.00135	316.9	8.2
Peyron granite 15D zircons										
15D/1	17	54	167	0.33	0.8689	0.0297	0.10176	0.00273	624.7	15.9
15D/2	37	33	671	0.05	0.4673	0.0145	0.05791	0.00153	362.9	9.3
15D/3	43	153	825	0.19	0.4068	0.0154	0.05101	0.00138	320.7	8.5
15D/4	110	86	1200	0.07	0.8201	0.0226	0.09773	0.00258	601.1	15.1
15D/5	72	357	732	0.49	0.7707	0.0218	0.09208	0.00243	567.8	14.3
15D/6	15	109	69	1.58	1.6572	0.0596	0.16402	0.00445	979.1	24.7
15D/7	60	168	922	0.18	0.5363	0.0162	0.06548	0.00173	408.9	10.5
15D/8	114	1074	928	1.16	0.8659	0.0240	0.10214	0.00270	626.9	15.7
15D/9	95	65	352	0.18	4.6483	0.1294	0.26166	0.00693	1498.3	35.4

Tab. 2 Continued

	Concentrations				Isotopic ratios				Age (Ma)	
Spot	**Pb ppm[1]**	**Th ppm[1]**	**U ppm[1]**	**Th/U**	**$^{207}Pb/^{235}U$[2]**	**± 2σ**	**$^{206}Pb/^{238}U$[2]**	**± 2σ**	**$^{206}Pb/^{238}U$**	**± 2σ**
15D/10	15	57	153	0.37	0.7822	0.0285	0.09343	0.00253	575.8	14.9
15D/11	35	68	341	0.20	0.9150	0.0275	0.10447	0.00278	640.5	16.2
15D/12	211	145	2871	0.05	0.6689	0.0184	0.07785	0.00205	483.3	12.3
15D/13	82	620	778	0.80	0.8375	0.0237	0.09519	0.00253	586.1	14.8
15D/14	69	856	295	2.90	1.5032	0.0436	0.14990	0.00398	900.4	22.3
15D/15	184	77	2149	0.04	0.8424	0.0238	0.09030	0.00240	557.3	14.2
15D/16	39	181	353	0.51	0.9134	0.0269	0.10523	0.00280	645.0	16.3
15D/17	70	494	673	0.73	0.8271	0.0236	0.09514	0.00253	585.8	14.9
15D/18	12	28	27	1.02	6.0881	0.1891	0.35389	0.00960	1953.2	45.7
15D/19	43	106	287	0.37	1.4502	0.0424	0.14815	0.00395	890.6	22.2
15D/20	31	328	255	1.29	0.8612	0.0264	0.10090	0.00270	619.7	15.8
15D/21	35	32	740	0.04	0.3928	0.0127	0.04993	0.00135	314.1	8.3
15D/22	20	90	174	0.52	1.3026	0.0408	0.09692	0.00263	596.3	15.4
15D/23	35	130	182	0.72	1.7461	0.0520	0.17303	0.00463	1028.8	25.5
15D/24	30	99	314	0.32	0.8046	0.0254	0.08800	0.00238	543.7	14.1
15D/25	23	97	193	0.50	0.9470	0.0296	0.11000	0.00295	672.8	17.2
15D/26	27	2	638	0.004	0.3425	0.0108	0.04674	0.00125	294.5	7.8
15D/27	19	129	141	0.92	1.1068	0.0367	0.11442	0.00310	698.3	18.0
15D/28	65	255	647	0.39	0.7999	0.0242	0.09583	0.00258	590.0	15.2
15D/29	98	222	1386	0.16	0.6243	0.0186	0.07218	0.00195	449.3	11.7
15D/30	53	147	557	0.26	0.8797	0.0268	0.09352	0.00253	576.3	14.9
15D/31	156	373	286	1.30	10.1131	0.2967	0.39389	0.01063	2140.8	49.2
15D/32	170	1609	1176	1.37	0.9649	0.0293	0.10911	0.00295	667.6	17.1
15D/33	169	718	1684	0.43	0.8371	0.0248	0.09611	0.00260	591.6	15.2
15D/34	126	272	941	0.29	1.2380	0.0366	0.13297	0.00358	804.8	20.4
15D/35	64	367	602	0.61	0.7997	0.0243	0.09645	0.00260	593.6	15.3
15D/36	58	220	564	0.39	0.8199	0.0250	0.09804	0.00265	602.9	15.6
Velay (Burzet) granite 20B monazites										
Mz20B/1	1660	61727	19090	3.2	0.3453	0.0109	0.04937	0.00153	310.6	9.4
Mz20B/2	1104	39585	13137	3.0	0.3442	0.0109	0.04931	0.00153	310.3	9.4
Mz20B/3	1432	48735	18117	2.7	0.3413	0.0107	0.04919	0.00153	309.6	9.4
Mz20B/4	1619	55927	19855	2.8	0.3477	0.0109	0.04989	0.00155	313.8	9.5
Mz20B/5	1233	53989	11615	4.6	0.3503	0.0113	0.04860	0.00150	305.9	9.3
Mz20B/6	1891	56498	27234	2.1	0.3561	0.0112	0.04905	0.00153	308.7	9.3
Mz20B/7	976	55273	4289	12.9	0.3505	0.0127	0.04956	0.00155	311.8	9.5
Mz20B/8	1647	59426	19794	3.0	0.3483	0.0110	0.04922	0.00153	309.7	9.4
Mz20B/9	1421	49279	17593	2.8	0.3453	0.0111	0.04928	0.00153	310.1	9.4
Mz20B/10	1255	47510	14559	3.3	0.3505	0.0114	0.04867	0.00150	306.4	9.3
Mz20B/11	1419	56117	14761	3.8	0.3553	0.0126	0.04814	0.00150	303.1	9.2
Mz20B/12	988	55089	4302	12.8	0.3486	0.0118	0.04958	0.00153	311.9	9.4
Mz20B/13	1292	53709	13084	4.1	0.3439	0.0112	0.04915	0.00153	309.3	9.3
Mz20B/14	1128	60466	6646	9.1	0.3583	0.0119	0.04919	0.00153	309.5	9.4
Mz20B/15	1269	66401	8085	8.2	0.3500	0.0124	0.04951	0.00155	311.5	9.5
Mz20B/16	1532	75071	11043	6.8	0.3543	0.0124	0.04980	0.00155	313.3	9.5
Mz20B/17	1602	50124	22211	2.3	0.3391	0.0111	0.04947	0.00153	311.3	9.4
Mz20B/18	990	64168	2923	22.0	0.3587	0.0143	0.04850	0.00153	305.3	9.4
Mz20B/19	1157	57582	7627	7.5	0.3416	0.0124	0.04898	0.00153	308.3	9.4
Mz20B/20	1676	72177	16283	4.4	0.3515	0.0118	0.04896	0.00153	308.2	9.3
Mz20B/21	1268	55663	11535	4.8	0.3423	0.0125	0.04895	0.00153	308.1	9.4
Mz20B/22	1656	78194	14240	5.5	0.3459	0.0117	0.04938	0.00153	310.7	9.4
Mz20B/23	2006	60256	30235	2.0	0.3403	0.0118	0.04816	0.00150	303.2	9.2
Peyron granite 15D monazites										
Mz15D/1	1188	35350	17609	2.0	0.3414	0.0117	0.04914	0.00153	309.2	9.3
Mz15D/2	847	30512	10643	2.9	0.3408	0.0119	0.04899	0.00153	308.3	9.3
Mz15D/3	1008	29916	14855	2.0	0.3409	0.0121	0.04894	0.00153	308.0	9.3
Mz15D/4	914	29722	12769	2.3	0.3458	0.0127	0.04908	0.00153	308.9	9.4
Mz15D/5	983	33743	12740	2.6	0.3447	0.0130	0.04895	0.00153	308.1	9.4

[1]: concentration uncertainty *c.* 20%

[2]: data not corrected for common Pb

Decay constants of Jaffrey et al. (1971) used

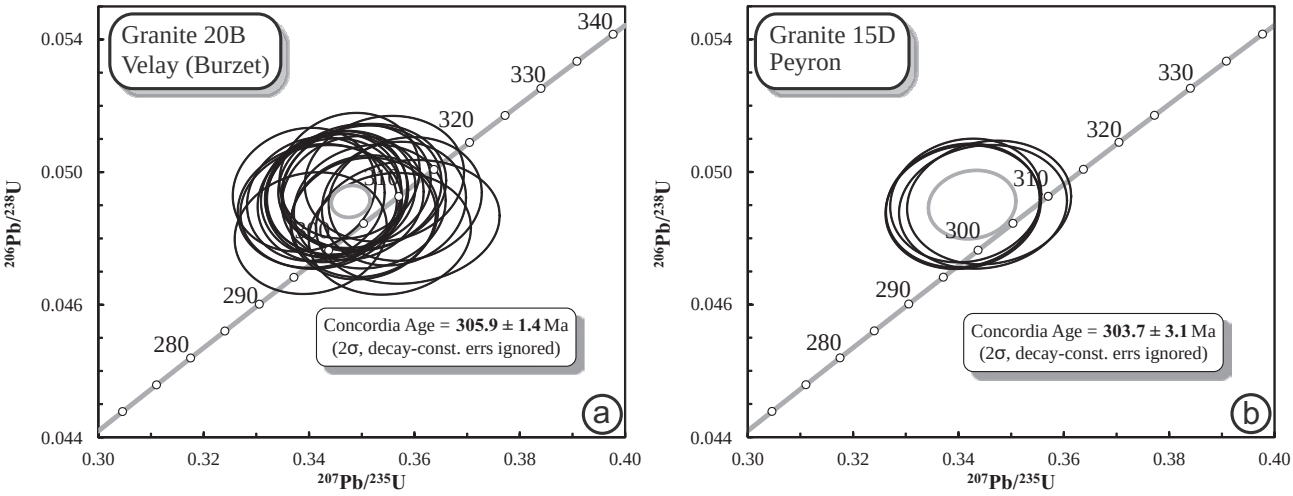

Fig. 5 Concordia diagrams for monazites in the Velay and Peyron granites.

sult of their very high U content, these metamict zircons may be systematically discordant and consequently the 294 Ma age would only be a minimum estimate. On the other hand, Pont-de-Bayzan is located close to the major La Souche Fault (Fig. 1) that also controlled the formation of the Stephanian Jaujac Basin (Weisbrod 1970). It can therefore be proposed that (a) this fault remained active until the Permian, draining the last mantle-derived magmas into the upper crust (see Scarrow et al. 2011). Indeed, the emplacement of at least some of the Pont-de-Bayzan bodies was clearly fault controlled (Fig. 2 and Appendix). Perhaps more likely, (b) the fault activity was associated with fluid circulation and perturbation of the isotopic system, an interpretation consistent with the scattering of the U–Pb data for this sample.

5.2. Host control on mafic magmas emplacement

In previous studies (Aït Malek 1997), the different shapes of vaugnerite bodies were considered to reflect successive magma batches and were used to discriminate between early, D_3-related, and late, D_4-related, intrusions. However, such an interpretation is not consistent with the undistinguishable within error ages obtained, regardless of the nature of the country rocks and degree of deformation of the vaugnerites. The various intrusions forms may be explained primarily by the contrasting rheological properties of the host. In partially molten systems, the melt fraction has a considerable impact on the rheology of the rock (e.g. Arzi 1978; Vigneresse et al. 2008; Vanderhaeghe 2009). Low-melt fraction systems behave as solids, whereas melt-rich rocks may attain a liquid-like rheology. In the Southern Velay, the vaugneritic intrusions are hosted by both migmatitic orthogneiss and paragneiss, which show evidence for

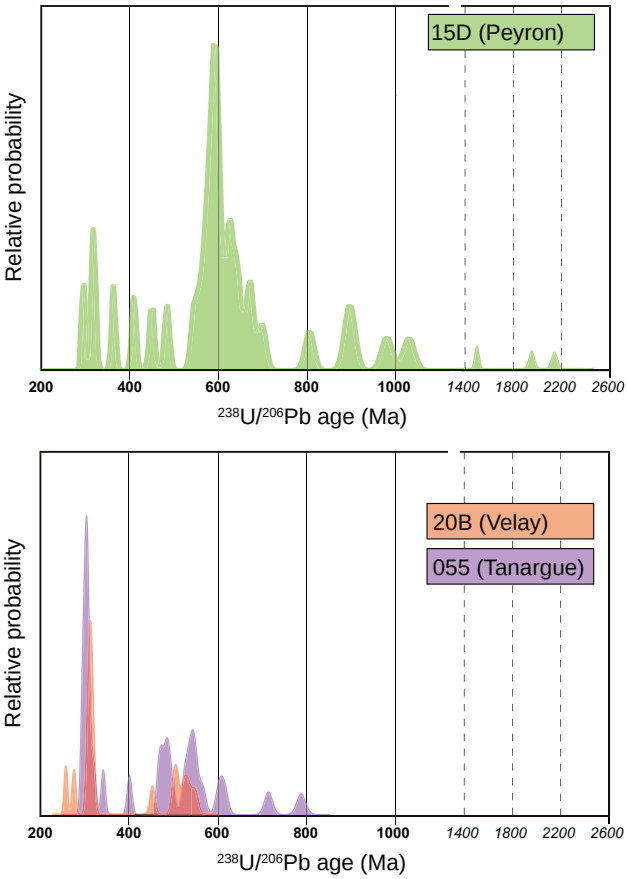

Fig. 6 Distribution of concordant and sub-concordant ages in the three peraluminous granites analysed: 15D (Peyron), top, 20B (Velay) and 55 (Tanargue), bottom. Note the scale break at 1000 Ma.

variable degree of anatexis, i.e. contrasting amounts of melt present. Vaugnerites hosted in low-melt fraction paragneisses or orthogneisses form sills or dyke swarms creeping in the migmatite melt network and mimicking the host foliation. In contrast, vaugnerites that intruded

into diatexitic paragneisses form round, apparently undeformed masses.

5.3. The source of Southern Velay granites

Although all the granites in our study area are nearly coeval, contrasting zircon inheritance patterns reveal that they were derived from distinct sources. The Peyron granite (a late phase of the Velay Complex) appears to have been generated from an old Cadomian crust, with a dominant *c.* 600 Ma peak (Fig. 6), as well as evidence for much older (early Proterozoic) components. Similar, early Proterozoic ages are known throughout the Massif Central in metasediments (see review in Melleton et al. 2010). Inherited ages of the Tanargue granite cluster at 540 and 470 Ma, corresponding to Cambrian and Ordovician magmatic events well known in the French Massif Central (e.g. R'Kha Chaham et al. 1990; Roger et al. 2004). The Velay granite proper shows a mostly Cambrian inheritance. By contrast, the Largentière granite shows no inheritance, suggesting that it originated from a juvenile protolith. Vaugnerites are likely to represent such a source since geochemical similarities suggest fractionation or remelting of newly emplaced Mg–K mafic rocks. Alternately, the (apparent) lack of inheritance could be a feature of the easy dissolution of high-U, likely metamict, zircons from the source; thereby providing a local U source allowing crystallization of Largentière granite's U-rich zircons (Schmidt et al. 2006). Thus, many parts of the Variscan crust experienced partial melting at the same time (305 Ma) leading to the production of granitic bodies from contrasting sources.

5.4. Long-lived crustal melting and catastrophic granite production

A compilation of U–Pb zircon and monazite magmatic ages available in the area (Fig. 7) shows that the great majority of granite plutons (excluding the early Rocles granite) were emplaced at around the same time. Both the late-granites from the Tanargue suite and the supposed "pre-Velay" Mont Lozère–Borne–Largentière granite intruded within the same short period as the main Velay granite, i.e. at *c.* 305 Ma.

However, the zircon age pattern of the Velay granite reveals the presence of Early Carboniferous zircons (~320 Ma), in addition to the older (source-related?) zircons (Fig. 6). This demonstrates that the main regional granitic event, the "M_4" HT crustal anatexis (Barbey et al. 1999; Ledru et al. 2001) followed a protracted period

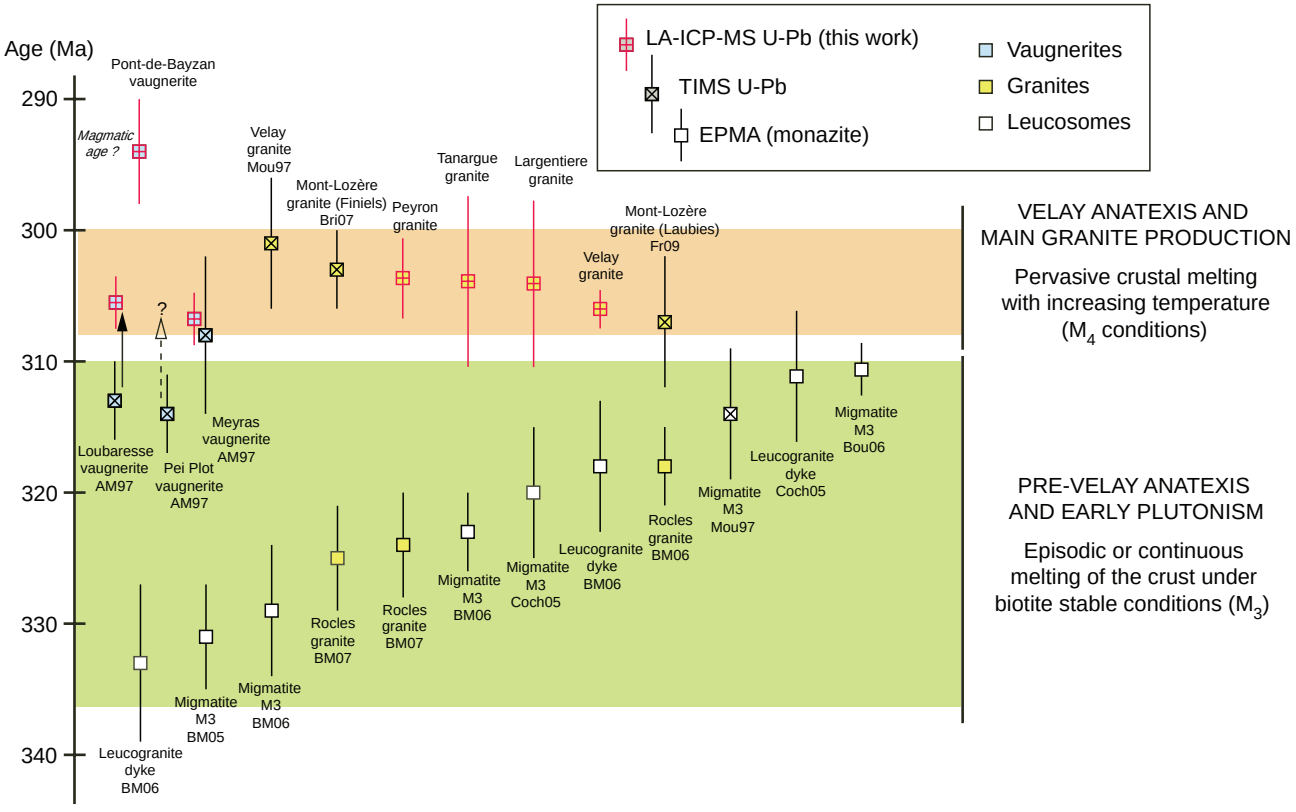

Fig. 7 Synthesis of U–Pb zircon (squares with symbols) and monazite (empty squares) ages with errors. Data sources: AM97: Ait Malek (1997); BM05: Be Mezeme et al. (2005); BM06: Be Mezeme et al. (2006); BM07: Be Mezeme et al. (2007); Bou06: Bouilhol et al. (2006); Bri07: Brichau et al. (2007); Coch05: Cocherie et al. (2005); Fr09: François (2009); Mou97: Mougeot et al. (1997). Red symbols: this study.

of pre-Velay (M_3) anatexis spanning between 335 and 310 Ma (Fig. 7). The M_3 event is recorded by the early "Velay" zircons, the Rocles granite (Be Mezeme et al. 2007) and the "low-temperature" (biotite stable; Montel et al. 1992) anatexis of the regional paragneisses (Mougeot et al. 1997; Be-Mezeme et al. 2005; Cocherie et al. 2005; Be Mezeme et al. 2006). Available data (Fig. 7) suggest that the M_3 melting was rather long-lived (> 20 Ma), but did not result in the formation of large granitic bodies; melt remained confined to migmatites and was rarely extracted and transferred into true plutons. A similar pattern has been described in other segments of the Variscan belt, such as Central Spain (Montero et al. 2004) or Calabria (Schenk 1990; Graessner et al. 2000), suggesting that this process occurred throughout the whole Variscan belt.

The M_3 and M_4 events, therefore, were very distinct. During M_3 anatexis, melt mostly remained trapped in its source. In contrast, during M_4, melt was extracted and collected in plutons. This difference most likely relates to temperature, which was some 50–100 °C higher during M_4. A higher temperature has two important consequences. Firstly, it results in a higher degree of anatexis that may be enough to bring the partially molten crust above the "Rheologically Critical Melt Percentage", (RCMP; Arzi 1978; Rosenberg 2001; Vigneresse and Burg 2004) above which the partially molten rocks behave as liquids, rather than solids. Secondly, the onset of biotite breakdown causes the disruption of the solid framework of melanosomes that holds the liquid in poorly connected leucosomes (Barraud et al. 2004). When these biotite-dominated layers collapse, the connectivity of the melt network suddenly increases, allowing melt extraction and formation of true plutons. Therefore, even the moderate heating at the M_3–M_4 transition may have been sufficient to cause a major shift in the overall mechanical behaviour of the crust.

5.5. Vaugnerites and the M_3–M_4 transition

The M_3–M_4 transition corresponded to moderate heating that resulted in an important rheological and tectonic change. The vaugnerites emplaced at this very moment and it is therefore clear that they are somehow related to this catastrophic process. Yet, their exact role remains unclear. Vaugnerites could be the actual cause: a sudden influx of mafic magmas in the already molten crust could have supplied enough heat to trigger the M_3–M_4 transition. Estimating the total volume of vaugnerites is difficult, because they crop out as rather common, but small, bodies. Therefore, it is hard to decide whether they are a volumetrically minor, or significant, component; and how much heat they could have transferred to the crust. Alternately, vaugnerites could just be the result of the same process that independently caused the heating of the crust: slab breakoff (Davies and von Blanckenburg 1995; van de Zedde and Wortel 2001; Atherton and Ghani 2002; Janoušek and Holub 2007), delamination of a lithospheric mantle root (Houseman et al. 1981; Houseman and Molnar 2001; Molnar and Houseman 2004) or orogenic collapse (England and Thompson 1984; Malavieille et al. 1990; Gardien et al. 1997; Rey et al. 2001; Vanderhaeghe and Teyssier 2001). All these processes would result in sudden heating of the crust, as well as concomitant generation of mafic melts (Arnold et al. 2001; Clark et al. 2011; Lexa et al. 2011).

5.6. The hot late Variscan crust

It is worth pointing out that M_4 corresponded to fairly extreme geothermal gradients: 800 °C for 2–5 kbar, i.e. 50–130 °C/km. It is, of course, totally unrealistic to extrapolate these gradients through the whole crust (as this would imply a Moho temperature greater than 1 500 °C). Therefore, the geotherm in the lower portions of the crust during M_4 times must have been much steeper, with a lower dT/dP. A similar "Z-shaped" geotherm has been advocated for "ultra-hot" orogens, such as those found in the Proterozoic or Archaean (Depine et al. 2008, Chardon et al. 2009). During at least a short period of its history, the Variscan belt was, in many respects, similar to such ultra-hot orogenic domains.

6. Conclusions

This work presents some of the first *in-situ* (LA-ICP-MS) ages for the southern French Massif Central granites and vaugnerites. Most of them were emplaced during a short time period at *c.* 305 Ma. This massive event of melting and catastrophic collapse of the orogenic crust followed a long-lived period (*c.* 20–30 Ma), during which the crust was partially molten but melts remained trapped and were not extracted to form granitic plutons. Crustal melting reached a climax at 305 Ma linked to a temperature increase that provoked biotite breakdown, thus leading to emplacement of the main cordierite-bearing Velay granite. This M_4 event of granite production was synchronous with intrusion of Mg–K mafic mantle-derived magmas in the middle crust. The catastrophic destabilization of the partially molten Variscan crust led to massive melt extraction from various crustal sources (older ortho- and paragneisses, newly emplaced vaugnerites), and so to the formation of numerous granitic plutons. It remains unclear whether the coeval Mg–K magmatism acted as a trigger for the eventual orogenic collapse or was just an expression of the HT regime. However, it is a key marker of the end of orogenic periods.

Acknowledgements. Pierre Bouilhol, Philippe-Hervé Leloup and Oscar Laurent are thanked for comments on earlier versions of this work and stimulating discussions. JHS was financially supported by the Spanish grant CGL2008–02864 and the Andalusian grant RNM1595. Reviews from Jean-Louis Vigneresse and František Holub helped to improve the quality of the manuscript. Editorial handling by Miroslav Štemprok and Vojtěch Janoušek was greatly appreciated.

Electronic supplementary material. The sample descriptions and locations are available online at the Journal web site *(http://dx.doi.org/10.3190/jgeosci.155).*

References

Aït Malek H (1997) Petrology, geochemistry and U/Pb geochronology of acid–basic associations: examples from SE Velay (French Massif Central) and western anti-Atlas (Morocco). Unpublished PhD thesis, University of Nancy, pp 1–297 (in French)

Alexandre P (2007) U–Pb zircon SIMS ages from the French Massif Central and implication for the pre-Variscan tectonic evolution in Western Europe. C R Geosci 339: 613–621

Arnold J, Jacoby W, Schmeling H, Schott B (2001) Continental collision and the dynamic and thermal evolution of the Variscan orogenic crustal root – numerical models. J Geodyn 31: 273–291

Arzi AA (1978) Critical phenomena in the rheology of partially melted rocks. Tectonophysics 44: 173–184

Atherton MP, Ghani AA (2002) Slab breakoff; a model for Caledonian, Late Granite syn-collisional magmatism in the orthotectonic (metamorphic) zone of Scotland and Donegal, Ireland. Lithos 62: 65-85

Barbey P, Marignac C, Montel JM, Macaudiere J, Gasquet D, Jabbori J (1999) Cordierite growth textures and the conditions of genesis and emplacement of crustal granitic magmas: the Velay granite Complex (Massif Central, France). J Petrol 40: 1425–1441

Barraud J, Gardien V, Allemand P, Grandjean P (2004) Analogue models of melt-flow networks in folding migmatites. J Struct Geol 26: 307–324

Be Mezeme E, Faure M, Cocherie A, Chen Y (2005) In situ chemical dating of tectonothermal events in the French Variscan Belt. Terra Nova 17: 420–426

Be Mezeme E, Cocherie A, Faure M, Legendre O, Rossi P (2006) Electron microprobe monazite geochronology of magmatic events: example from Variscan migmatites and granitoids, Massif Central, France. Lithos 87: 276–288

Be Mezeme E, Faure M, Chen Y, Cocherie A, Talbot JY (2007) Structural, AMS and geochronological study of a laccolith emplaced during Late Variscan orogenic extension: the Rocles Pluton (SE French Massif Central). Int J Earth Sci 96: 215–228

Bea F, Montero P, Ortega M (2006) A LA–ICP–MS evaluation of Zr reservoirs in common crustal rocks: implications for Zr and Hf geochemistry, and zircon-forming processes. Canad Mineral 44: 693–714

Berger J, Féménias O, Ohnenstetter D, Bruguier O, Plissart G, Mercier JCC, Demaiffe D (2010) New occurrence of UHP eclogites in Limousin (French Massif Central): age, tectonic setting and fluid–rock interactions. Lithos 118: 365–382

Bonin B (2004) Do coeval mafic and felsic magmas in post-collisional to within-plate regimes necessarily imply two contrasting, mantle and crustal, sources? A review. Lithos 78: 1–24

Bouilhol P, Leyreloup AF, Delor C, Vauchez A, Monié P (2006) Relationships between lower and upper crust tectonic during doming: the mylonitic southern edge of the Velay metamorphic core complex (Cévennes – French Massif Central). Geodin Acta 19: 137–153

Bowes D, Košler J (1993) Geochemical comparison of the subvolcanic appinite suite of the British Caledonides and the durbachite suite of the Central European Hercynides: evidence for associated shoshonitic and granitic magmatism. Mineral Petrol 48: 47–63

Brichau S, Respaut JP, Monié P (2008) New age constraints on emplacement of the Cévenol granitoids, South French Massif Central. Int J Earth Sci 97: 725–738

Caen-Vachette M, Couturié J, Didier J (1982) Radiometric ages of anatectic and late-migmatitic Velay granites (French Massif Central). C R Acad Sci Paris 294: 135–138 (in French)

Caron C (1994) Pb–Zn mineralizations in the lower Paleozoic of southern Europe. Isotopic Pb study of Iglesiente (SW Sardaigne) and Cévennes mineral deposits, and evolution of the country rocks using U–Pb, Ar–Ar and K–Ar geochronology. Unpublished PhD thesis, University of Montpellier, pp 1–288 (in French)

Castro A, Corretgé LG, De la Rosa J, Fernández C, López S, García-Moreno O, Chacón H (2003) The Appinite-Migmatite Complex of Sanabria, NW Iberian Massif, Spain. J Petrol 44: 1309–1344

Chardon D, Gapais D, Cagnard F (2009) Flow of ultra-hot orogens: a view from the Precambrian, clues for the Phanerozoic. Tectonophysics 477: 105–118

Clark C, Fitzsimons ICW, Healy D, Harley SL (2011) When the continental crust melts: how does the continental crust get really hot? Elements 7: 235–240

Cocherie A, Mezeme EB, Legendre O, Fanning CM, Faure M, Rossi P (2005) Electron-microprobe dating as a tool for determining the closure of Th–U–Pb systems in migmatitic monazites. Amer Miner 90: 607–618

Costa S, Rey P (1995) Lower crustal rejuvenation and growth during post-thickening collapse: insights from

a crustal cross section through a Variscan metamorphic core complex. Geology 23: 905

Davies JH, von Blanckenburg F (1995) Slab breakoff: a model of lithosphere detachment and its test in the magmatism and deformation of collisional orogens. Earth Planet Sci Lett 129: 85–102

Depine GV, Andronicos CL, Phipps-Morgan J (2008) Near-isothermal conditions in the middle and lower crust induced by melt migration. Nature 452: 80–83

Didier A, Bosse V, Boulvais P, Bouloton J, Paquette JL, Montel JM, Devidal JL (2013) Disturbance versus preservation of U–Th–Pb ages in monazite during fluid–rock interaction: textural, chemical and isotopic in situ study in microgranites (Velay Dome, France). Contrib Mineral Petrol 165: 1051–1072

Didier J, Azelarab ELM, Fernandez A (1987) Interactions between a diorite magma and a palingenetic granitic magma at the Peyron, near Burzet (Ardèche, French Massif Central). C R Acad Sci Paris 304: 1227–1232 (in French)

Downes H, Shaw A, Williamson BJ, Thirlwall MF (1997) Sr, Nd and Pb isotopic evidence for the lower crustal origin of Hercynian granodiorites and monzogranites, Massif Central, France. Chem Geol 140: 289–289

Ducrot J, Lancelot JR, Marchand J (1983) U–Pb dating on zircons on La-Borie eclogite (Haut-Allier, France) and consequences on the Ante-Hercynian evolution of Occidental Europe. Earth Planet Sci Lett 62: 385–394

Edel JB (2001) The rotations of the Variscides during the Carboniferous collision: paleomagnetic constraints from the Vosges and the Massif Central (France). Tectonophysics 332: 69–92

England PC, Thompson AB (1984) Pressure–temperature–time paths of regional metamorphism, part I: heat transfer during the evolution of regions of thickened continental crust. J Petrol 25: 894–928

Faure M, Lardeaux JM, Ledru P (2009) A review of the pre-Permian geology of the Variscan French Massif Central. C R Geosci 341: 202–213

Fowler MB (1988) Ach'uaine hybrid appinite pipes – evidence for mantle-derived shoshonitic parent magmas in Caledonian granite genesis. Geology 16: 1026–1030

Fowler M, Rollinson H (2012) Phanerozoic sanukitoids from Caledonian Scotland: implications for Archean subduction. Geology 40: 1079–1082

Fowler M, Kocks H, Darbyshire D, Greenwood P (2008) Petrogenesis of high Ba–Sr plutons from the Northern Highlands Terrane of the British Caledonian Province. Lithos 105: 129–148

François T (2009) Geochemical and geochronological constraints on the origin and emplacement of Mont-Lozère granites. Unpublished MSci., University of Montpellier, pp 1–39 (in French)

Gagny C (1979) Vaugnerites and durbachites are cumulates derived from a granitic magma (example of the Crêtes magma, Vosges). C R Acad Sci Paris 287: 1361–1364 (in French)

Gardien V, Lardeaux JM, Ledru P, Allemand P, Guillot S (1997) Metamorphism during late orogenic extension: insights from the French Variscan belt. Bull Soc Geol Fr 168: 271–286

Gasquet D, Bertrand JM, Paquette JL, Lehmann J, Ratzov G, Guedes RDA, Tiepolo M, Boullier AM, Scaillet S, Nomade S (2010) Miocene to Messinian deformation and hydrothermal activity in a pre-Alpine basement massif of the French western Alps: new U–Th–Pb and argon ages from the Lauzière Massif. Bull Soc Geol Fr 181: 227–241

Gerdes A, Wörner G, Finger F (2000) Hybrids, magma mixing and enriched mantle melts in post-collisional Variscan granitoids: the Rastenberg Pluton, Austria. In: Franke W, Haak V, Oncken O, Tanner D (eds) Orogenic Processes: Quantification and Modelling in the Variscan Belt. Geological Society London Special Publications 179: pp 415–431

Graessner T, Schenk V, Bröcker M, Mezger K (2000) Geochronological constraints on the timing of granitoid magmatism, metamorphism and post-metamorphic cooling in the Hercynian crustal cross-section of Calabria. J Metamorph Geol 18: 409–421

Guy A, Edel JB, Schulmann K, Tomek Č, Lexa O (2011) A geophysical model of the Variscan orogenic root (Bohemian Massif): implications for modern collisional orogens. Lithos 124: 144–157

Holub FV (1997a) Trace-element patterns in ultrapotassic rocks of the Bohemian Massif: implications for heterogeneity of their mantle sources. J Czech Geol Soc 42: 9

Holub FV (1997b) Ultrapotassic plutonic rocks of the durbachite series in the Bohemian Massif: petrology, geochemistry and petrogenetic interpretation. Sbor geol věd, Ložisk geol mineral 31: 5–26

Houseman G, McKenzie D, Molnar P (1981) Convective instability of a thickened boundary layer and its relevance for the thermal evolution of continental convergent belts. J Geophys Res 86: 6115–6132

Houseman G, Molnar P (2001) Mechanisms of lithospheric rejuvenation associated with continental orogeny. In: Miller JA, Holdsworth RE, Buick IS, Hand M (eds) Continental Reactivation and Reworking. Geological Society London Special Publications 184: pp 13–38

Hurai V, Paquette JL, Huraiová M, Konečný P (2010) U–Th–Pb geochronology of zircon and monazite from syenite and pincinite xenoliths in Pliocene alkali basalts of the intra-Carpathian back-arc basin. J Volcanol Geotherm Res 198: 275–287

Jackson SE, Pearson NJ, Griffin WL, Belousova EA (2004) The application of laser ablation-inductively coupled plasma-mass spectrometry to in situ U–Pb zircon geochronology. Chem Geol 211: 47–69

Jaffrey AH, Flynn KF, Glendenin LE, Bentley WC, Essling AM (1971) Precision measurement of half-lives and specific activities of ^{235}U and ^{238}U. Phys Rev C4:1889–1906

Janoušek V, Holub FV, Rogers G, Bowes D (1997) Two distinct mantle sources of Hercynian magmas intruding the Moldanubian unit, Bohemian Massif, Czech Republic. J Czech Geol Soc 42: 10

Janoušek V, Holub FV (2007) The causal link between HP–HT metamorphism and ultrapotassic magmatism in collisional orogens: case study from the Moldanubian Zone of the Bohemian Massif. Proc Geol Assoc 118: 75–86

Kober B, Lippolt HJ (1985) Pre-Hercynian mantle lead transfer to basement rocks as indicated by lead isotopes of the Schwarzwald crystalline, SW-Germany. Contrib Mineral Petrol 90: 162–171

Kotková J, Leichmann J, Schaltegger U (2003) 338–335 Ma old intrusions in the E Bohemian massif – a relic of the orogen-wide durbachitic magmatism in European Variscides. J Czech Geol Soc 48: 80–81

Kotková J, Leichmann J, Schaltegger U (2010) Two types of ultrapotassic plutonic rocks in the Bohemian Massif – coeval intrusions at different crustal levels. Lithos 115: 163–176

Kroner U, Romer RL (2013) Two plates – many subduction zones: the Variscan orogeny reconsidered. Gondwana Res 24: 298–329

Lagarde JL, Dallain C, Ledru P, Courrioux G (1994) Strain patterns within the late Variscan granitic dome of Velay, French Massif Central. J Struct Geol 16: 839–852

Lardeaux JM, Ledru P, Daniel I, Duchene S (2001) The Variscan French Massif Central – a new addition to the ultrahigh pressure metamorphic 'club': exhumation processes and geodynamic consequences. Tectonophysics 332: 143–167

Ledru P, Courrioux G, Dallain C, Lardeaux JM, Montel JM, Vanderhaeghe O, Vitel G (2001) The Velay Dome (French Massif Central): melt generation and granite emplacement during orogenic evolution. Tectonophysics 342: 207–237

Lexa O, Schulmann K, Janoušek V, Štípská P, Guy A, Racek M (2011) Heat sources and trigger mechanisms of exhumation of HP granulites in Variscan orogenic root. J Metamorph Geol 29: 79–102

Ludwig K (2008) User's manual for Isoplot Version 3.70, a geochronological toolkit for Microsoft Excel. Berkeley Geochronology Center Special Publications 4: 1–76

Malavieille JP, Guihot P, Costa S, Lardeaux JM, Gardien V (1990) Collapse of the thickened Variscan crust in the French Massif Central: Mont Pilat extensional shear zone and St Etienne Late Carboniferous basin. Tectonophysics 177: 139–149

Marignac C, Leroy J, Macaudiere J (1980) Tectonometamorphic evolution of a part of the Hercynian orogen – the Cévennes médianes, French Massif Central. C R Acad Sci Paris 291: 605–608 (in French)

Martin H, Moyen JF, Rapp R (2010) Sanukitoids and the Archaean–Proterozoic boundary. Trans Roy Soc Edinb, Earth Sci 100: 15–33

Matte P (1986) Tectonics and plate-tectonics model for the Variscan Belt of Europe. Tectonophysics 126: 329–374

Melleton J, Cocherie A, Faure M, Rossi P (2010) Precambrian protoliths and Early Paleozoic magmatism in the French Massif Central: U–Pb data and the North Gondwana connection in the west European Variscan belt. Gondwana Res 17: 13–25

Mialhe J (1980) The Borne granite, petrographic geochemical and geochronological study. Unpublished PhD thesis, University of Clermont, pp 1–171 (in French)

Michon G (1987) Vaugnerites from eastern French Massif Central: a multivariate statistical approach on major elements. Bull Soc Géol France 3: 591–600 (in French)

Molina JF, Montero P, Bea F, Scarrow JH (2012) Anomalous xenocryst dispersion during tonalite–granodiorite crystal mush hybridization in the mid crust: mineralogical and geochemical evidence from Variscan appinites (Avila Batholith, Central Iberia). Lithos 153: 224–242

Molnar P, Houseman G (2004) The effects of buoyant crust on the gravitational instability of thickened mantle lithosphere at zones of intracontinental convergence. Geophys J Int 158: 1134–1150

Montel JM (1988) First discovery of an orthopyroxene-bearing vaugnerite: petrography, geochemistry, and implications on the genesis of vaugnerites. C R Acad Sci Paris 306: 985–990 (in French)

Montel JM, Abdelghaffar R (1993) Late-migmatitic granites from the Velay (Massif Central): main petrographic and geochemical characteristics. Géol Fr 1: 15–28 (in French)

Montel JM, Weisbrod A (1986) Characteristics and evolution of "vaugneritic magmas": an analytical and experimental approach, on the example of the Cévennes Médianes (French Massif Central). Bull Minéral 109: 575–587

Montel JM, Marignac C, Barbey P, Pichavant M (1992) Thermobarometry and granite genesis – the Hercynian low-P, high-T Velay anatectic dome (French Massif-Central). J Metamorph Geol 10: 1–15

Montero P, Bea F, Zinger T, Scarrow J, Molina J, Whitehouse M (2004) 55 million years of continuous anatexis in Central Iberia: single-zircon dating of the Peña Negra Complex. J Geol Soc, London 161: 255–263

Mougeot R, Respaut JP, Ledru P, Marignac C (1997) U–Pb chronology on accessory minerals of the Velay anatectic dome (French Massif Central). Eur J Mineral 9: 141–156

Murphy JB (2013) Appinite suites: a record of the role of water in the genesis, transport, emplacement and crystallization of magma. Earth Sci Rev 119: 35–59

Palm QA (1957) Crystalline rocks from the Cévennes médianes, near Largentière, Ardèche, France. Unpublished PhD thesis, University of Utrecht, pp 1–121 (in French)

Paquette JL, Monchoux P, Couturier M (1995) Geochemical and isotopic study of a norite–eclogite transition in the European Variscan belt: implications for U–Pb zircon systematics in metabasic rocks. Geochim Cosmochim Acta 59: 1611–1622

Perini G, Cebria J, López-Ruiz J, Doblas M (2004) Carboniferous–Permian mafic magmatism in the Variscan belt of Spain and France: implications for mantle sources. In: Wilson M, Neumann ER, Davies GR, Timmerman MJ, Heeremans M, Larsen BT (eds) Permo–Carboniferous Magmatism and Rifting in Europe. Geological Society London Special Publications 223: pp 415–438

Pin C, Lancelot J (1982) U–Pb dating of an early Paleozoic bimodal magmatism in the French Massif Central and of its further metamorphic evolution. Contrib Mineral Petrol 79: 1–12

Pin C, Marini F (1993) Early Ordovician continental break-up in Variscan Europe: Nd–Sr isotope and trace element evidence from bimodal igneous associations of the Southern Massif Central, France. Lithos 29: 177–196

R'Kha Chaham K, Couturié JP, Duthou JL, Fernandez A, Vitel G (1990) The Fix augen gneiss (French Massif Central): a new evidence for the lower Cambrian peraluminous magmatism. C R Acad Sci Paris 311: 845–850 (in French)

Rey P, Vanderhaeghe O, Teyssier C (2001) Gravitational collapse of the continental crust : definition, regimes and modes. Tectonophysics 342: 435–449

Roger F, Respaut JP, Brunel M, Matte P, Paquette JL (2004) U–Pb dating of Augen orthogneisses from the Axial Zone of the Montagne Noire (southern of Massif Central): new witness of Ordovician magmatism into the Variscan Belt. C R Geosci 336: 19–28

Rosenberg CL (2001) Deformation of partially molten granite: a review and comparison of experimental and natural case studies. Int J Earth Sci 90: 60–76

Sabatier H (1980) Vaugnérites and granites, a peculiar association of basic and acid rocks. Bull Minéral 103: 507–522

Sabatier H (1991) Vaugnerites: special lamprophyre-derived mafic enclaves in some Hercynian granites from Western and Central Europe. In: Didier J, Barbarin B (eds) Enclaves and Granite Petrology. Elsevier, Amsterdam, pp 63–81

Scarrow JH, Bea F, Montero P, Molina J (2008) Shoshonites, vaugnerites and potassic lamprophyres: similarities and differences between 'ultra'-high-K rocks. Trans Roy Soc Edinb, Earth Sci 99: 159–175

Scarrow JH, Molina J, Bea F, Montero P (2009) Within-plate calc-alkaline rocks: insights from alkaline mafic magma – peraluminous crustal melt hybrid appinites of the Central Iberian Variscan continental collision. Lithos 110: 50–64

Scarrow JH, Molina JF, Bea F, Montero P, Vaughan APM (2011) Lamprophyre dikes as tectonic markers of late orogenic transtension timing and kinematics: a case study from the Central Iberian Zone. Tectonics 30: TC4007

Schenk V (1990) The exposed crustal cross section of southern Calabria, Italy: structure and evolution of a segment of Hercynian crust. In: Salisbury MH, Fountain DM (eds) Exposed Cross-Sections of the Continental Crust. Springer, New York, pp 21–42

Schmidt C, Rickers K, Wirth R, Nasdala L, Hanchar JM (2006) Low-temperature Zr mobility: an in situ synchrotron-radiation XRF study of the effect of radiation damage in zircon on the element release in H_2O + HCl ± SiO_2 fluids. Amer Miner 91: 1211–1215

Tera F, Wasserburg G (1972) U–Th–Pb systematics in three Apollo 14 basalts and the problem of initial Pb in lunar rocks. Earth Planet Sci Lett 14: 281–304

van de Zedde DMA, Wortel MJR (2001) Shallow slab detachment as a transient source of heat at midlithospheric depths. Tectonics 20: 868–882

Vanderhaeghe O, Teyssier C (2001) Crustal-scale rheological transitions during late-orogenic collapse. Tectonophysics 335: 211–228

Vanderhaeghe O (2009) Migmatites, granites and orogeny: flow modes of partially-molten rocks and magmas associated with melt/solid segregation in orogenic belts. Tectonophysics 477: 119–134

Vigneresse JL, Burg JP (2004) Strain-rate dependent rheology of partially molten rocks. In: Grocott J, McCaffrey KJW, Taylor G, Tikoff B (eds) Vertical Coupling and Decoupling in the Lithosphere. Geological Society London Special Publications 227: pp 327–336

Vigneresse JL, Burg JP, Moyen JF (2008) Instabilities development in partially molten rocks. Boll Soc geol ital 127: 235–242

von Raumer JF, Stampfli GM, Bussy F (2003) Gondwana-derived microcontinents – the constituents of the Variscan and Alpine collisional orogens. Tectonophysics 365: 7–22

Weisbrod A (1970) Petrology of the metamorphic basement in the Cévennes Médianes (French Massif Central): sedimentological reconstruction and thermodynamic study of metamorphism. Unpublished thesis, University of Nancy, pp 1–244

Williamson BJ, Downes H, Thirlwall MF (1992) The relationship between crustal magmatic underplating and granite genesis – an example from the Velay granite complex, Massif Central, France. Trans Roy Soc Edinb, Earth Sci 83: 235–245